Electronic Supplementary Material (ESI) for Journal of Materials Chemistry A.

Supplementary Materials for

Synthesis of metal cation doped nanoparticles for single atom alloy catalysts using spontaneous cation exchange

Xiangyun Xiao[a,b‡], Sungsu Kang[c,d‡], Seokhyun Choung[e‡], Jeong Woo Han[e*], Jungwon Park[c,d,f,g*]& Taekyung Yu[a*]

[a]Department of Chemical Engineering, College of Engineering, Integrated Engineering Major, Kyung Hee University, Yongin 17104, Korea.

[b]Faculty of Materials Science and Engineering/Institute of Technology for Carbon Neutrality, Shenzhen Institute of Advanced Technology (SIAT), Chinese Academy of Sciences (CAS), Shenzhen, 518055 P. R. China.

[c]School of Chemical and Biological Engineering, Institute of Chemical Process, Seoul National University, Seoul 08826, South Korea.

[d]Center for Nanoparticle Research, Institute for Basic Science (IBS), Seoul 08826, South Korea.

[e]Department of Chemical Engineering, Pohang University Science and Technology (POSTECH); Pohang, Gyeongbuk 37673, Republic of Korea.

[f]Institute of Engineering Research, Seoul National University, Seoul 08826, South Korea.

[g]Advanced Institutes of Convergence Technology, Seoul National University, Seoul 08826, South Korea.

Contact E-mail: jwhan@postech.ac.kr; jungwonpark@snu.ac.kr; tkyu@khu.ac.kr

‡Those authors contribute equally to this paper.

This Supplementary Information contains:

Supplementary Figures 1-46

Supplementary Tables 1-10

Supplementary Note

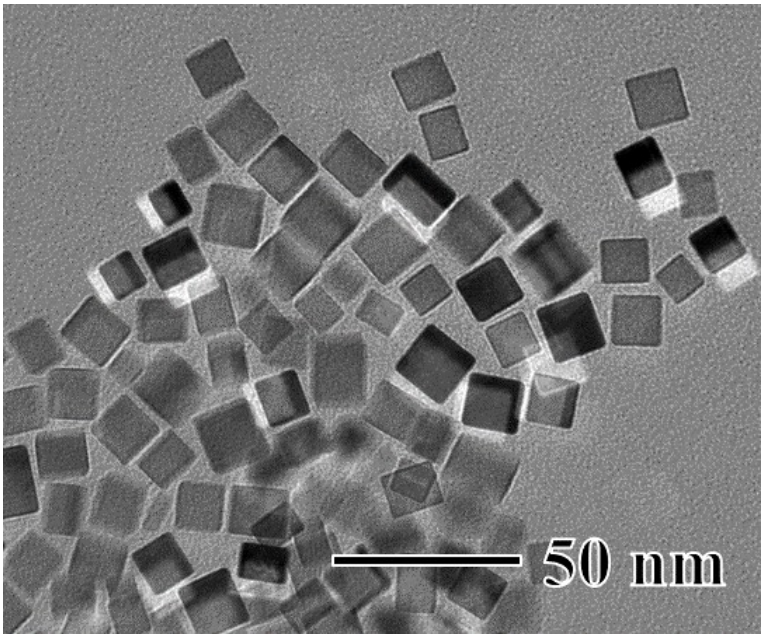

Fig. S1. TEM images of the Pd nanocubes.

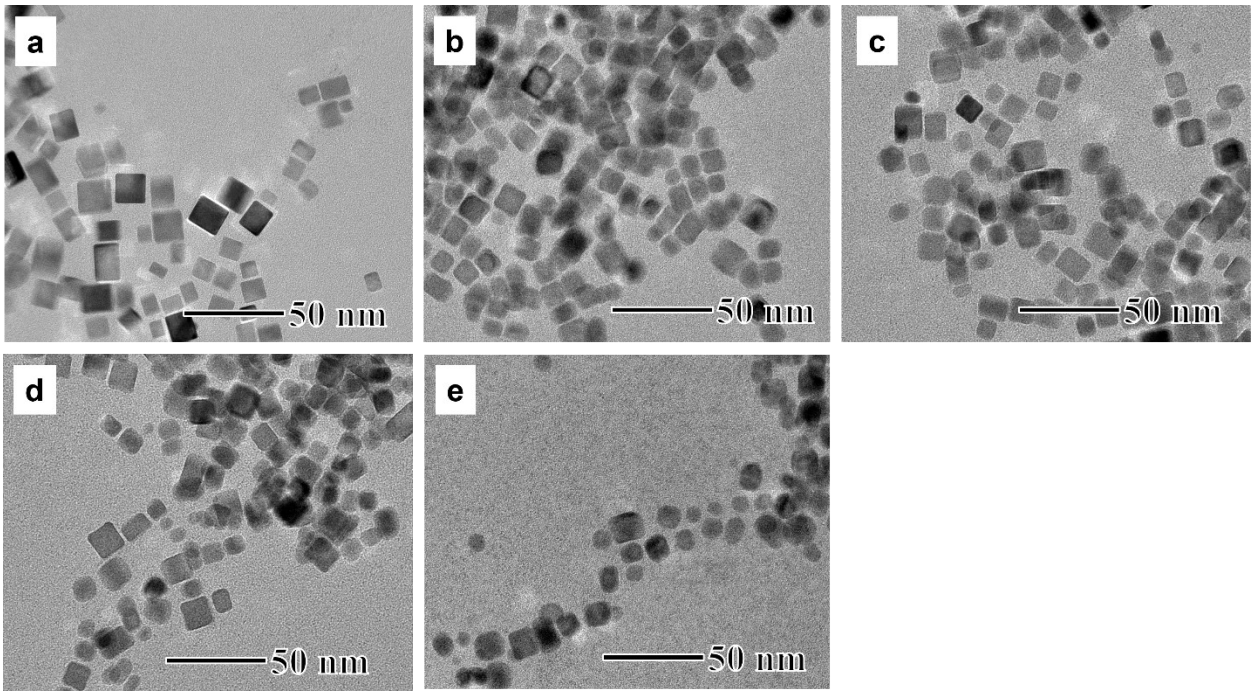

Fig. S2. TEM images of $PdRu_1$ (a), $PdRu_{20}$ (b), $PdRu_{40}$ (c), $PdRu_{60}$ (d), and $PdRu_{100}$ (e) nanocubes after the reaction time of 3 h.

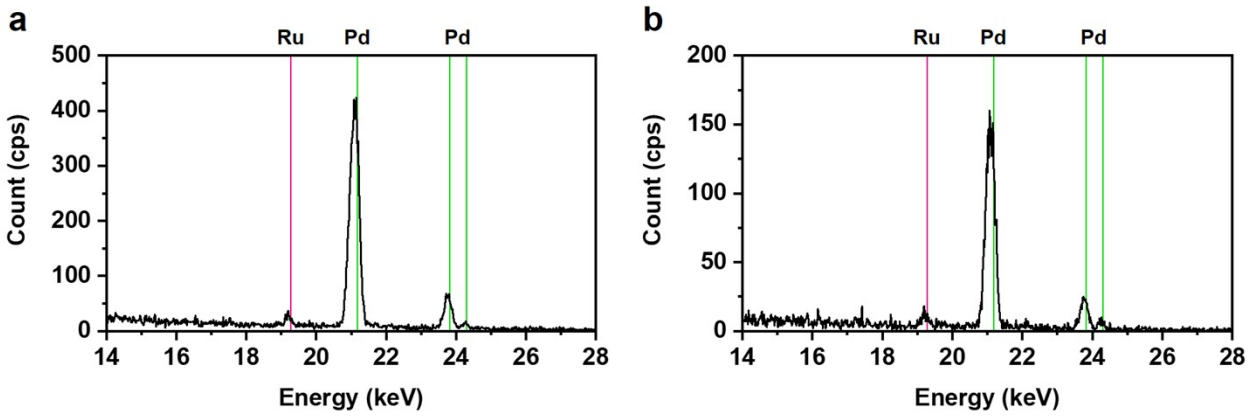

Fig. S3. EDS spectra of the $PdRu_{20}$. (a) EDS spectrum corresponds to the EDS line scan presented in Fig 1b and 1c in the main text. (b) EDS spectrum corresponds to the EDS maps presented in Fig 1d in the main text.

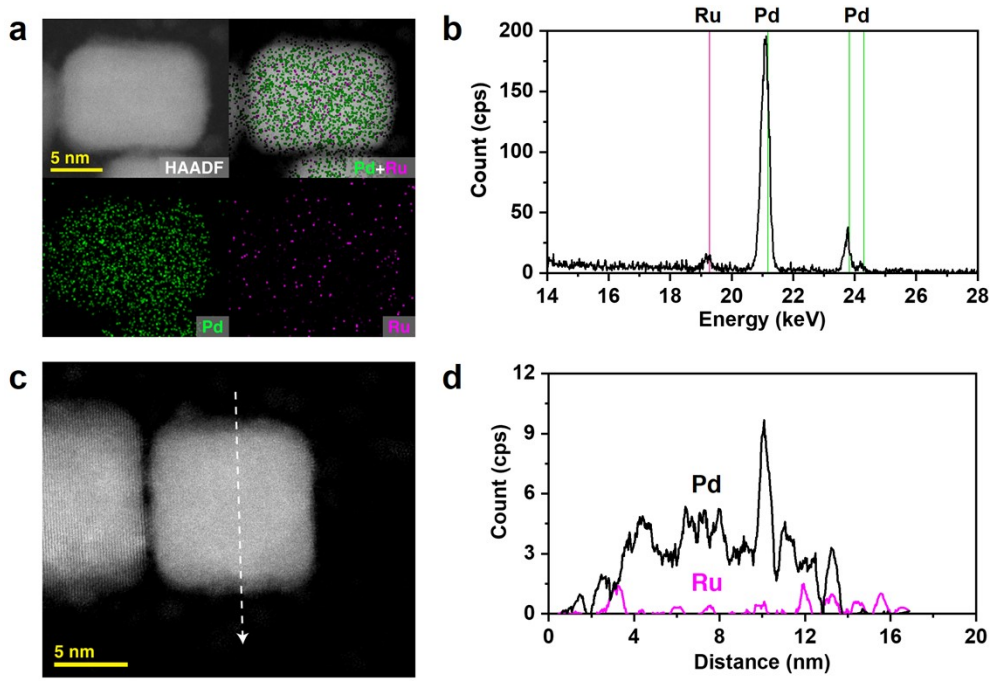

Fig. S4. Additional STEM-EDS analyses of the $PdRu_{20}$. (a and b) HAADF-STEM images and EDS elemental maps (a), and corresponding EDS spectrum (b) of the $PdRu_{20}$. (c and d) HAADF-STEM images and EDS line profiles for Pd and Ru (c) and corresponding EDS spectrum (d) of the $PdRu_{20}$.

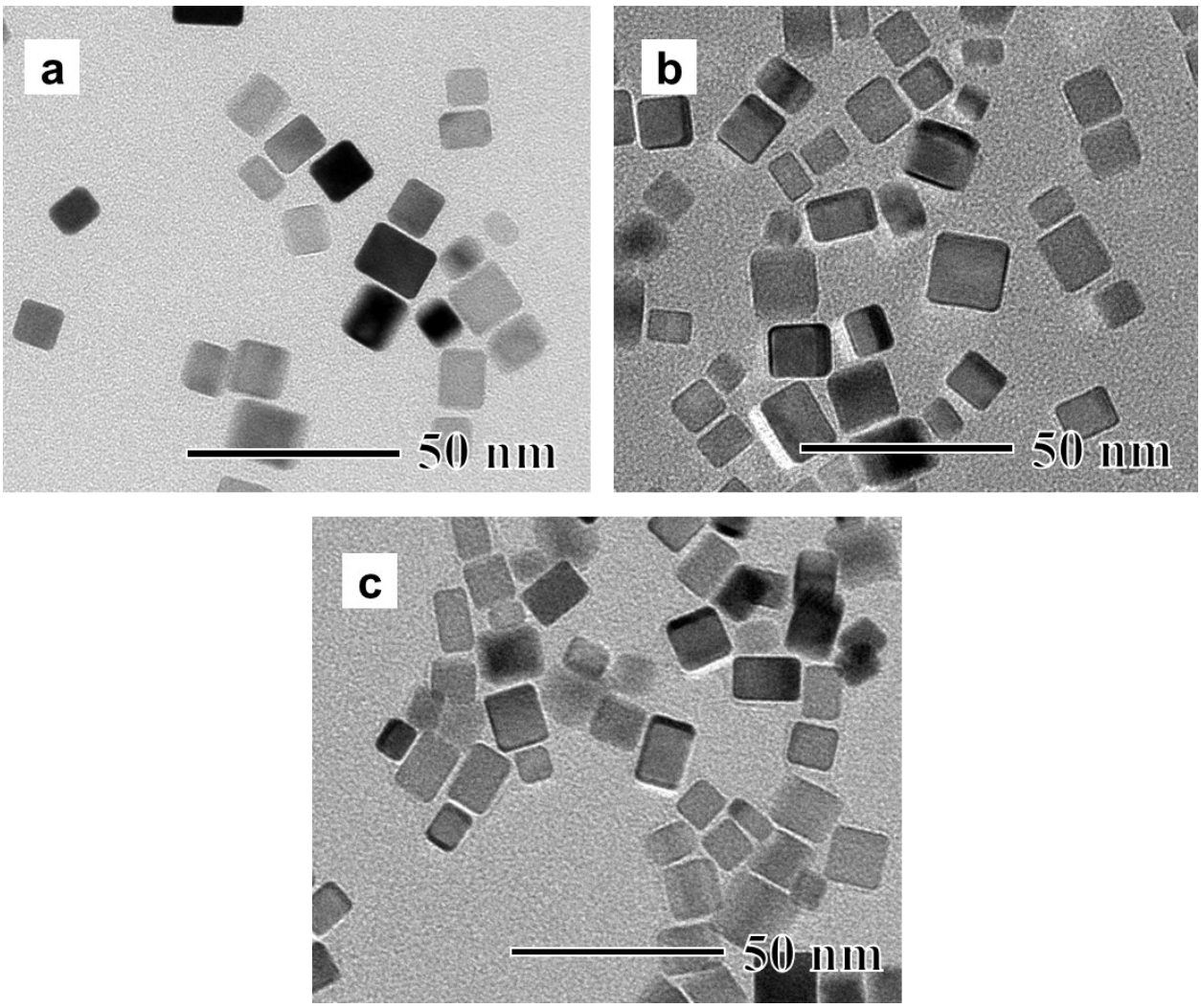

Fig. S5. The TEM images of Pd@Ru with different Ru ratio (a) m_{Ru}/m_{Pd}=1%, (b) m_{Ru}/m_{Pd}=20%, (c) m_{Ru}/m_{Pd}=40%.

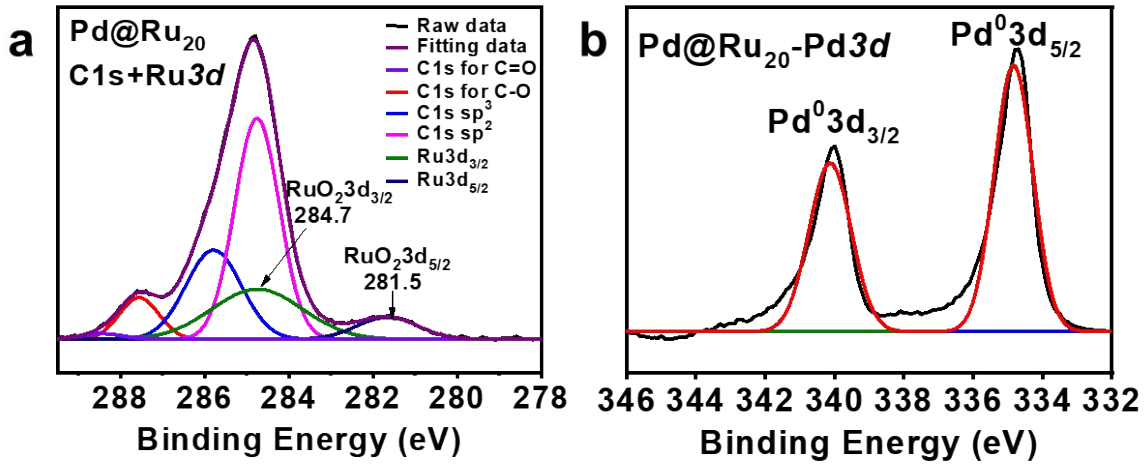

Fig. S6. (a) Ru3d with C1s XPS pattern of Pd@Ru_{20}. (b) Pd 3d XPS patterns of Pd@Ru_{20}.

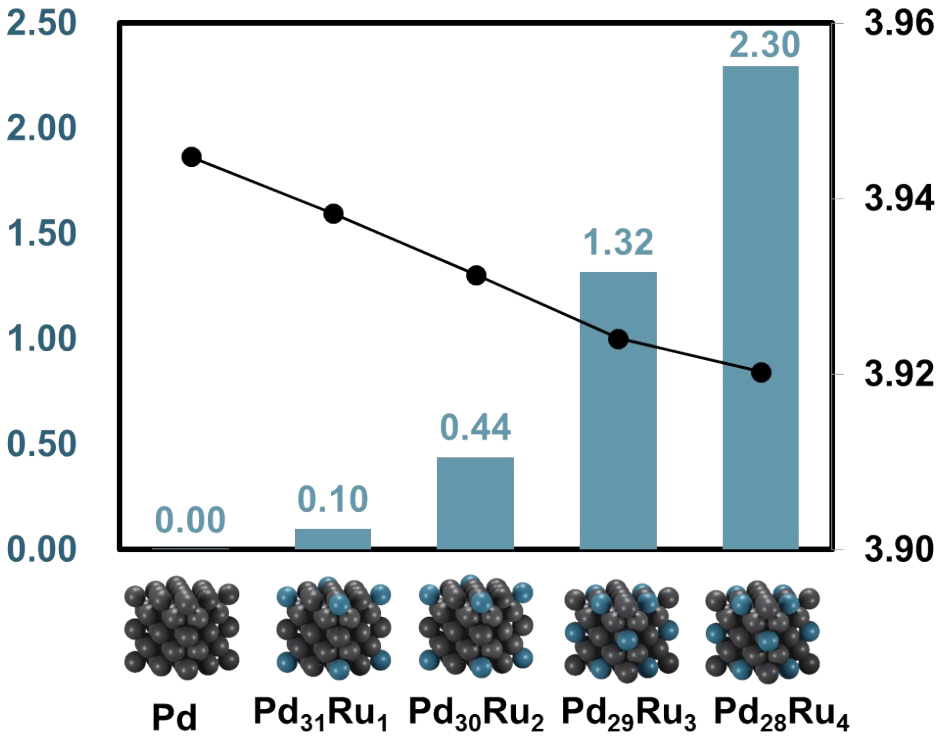

Fig. S7. Bulk alloy formation energy of $Pd_{32-x}Ru_x$ alloys (x = 0 ~ 4). (Color code: Pd: gray and Ru: blue)

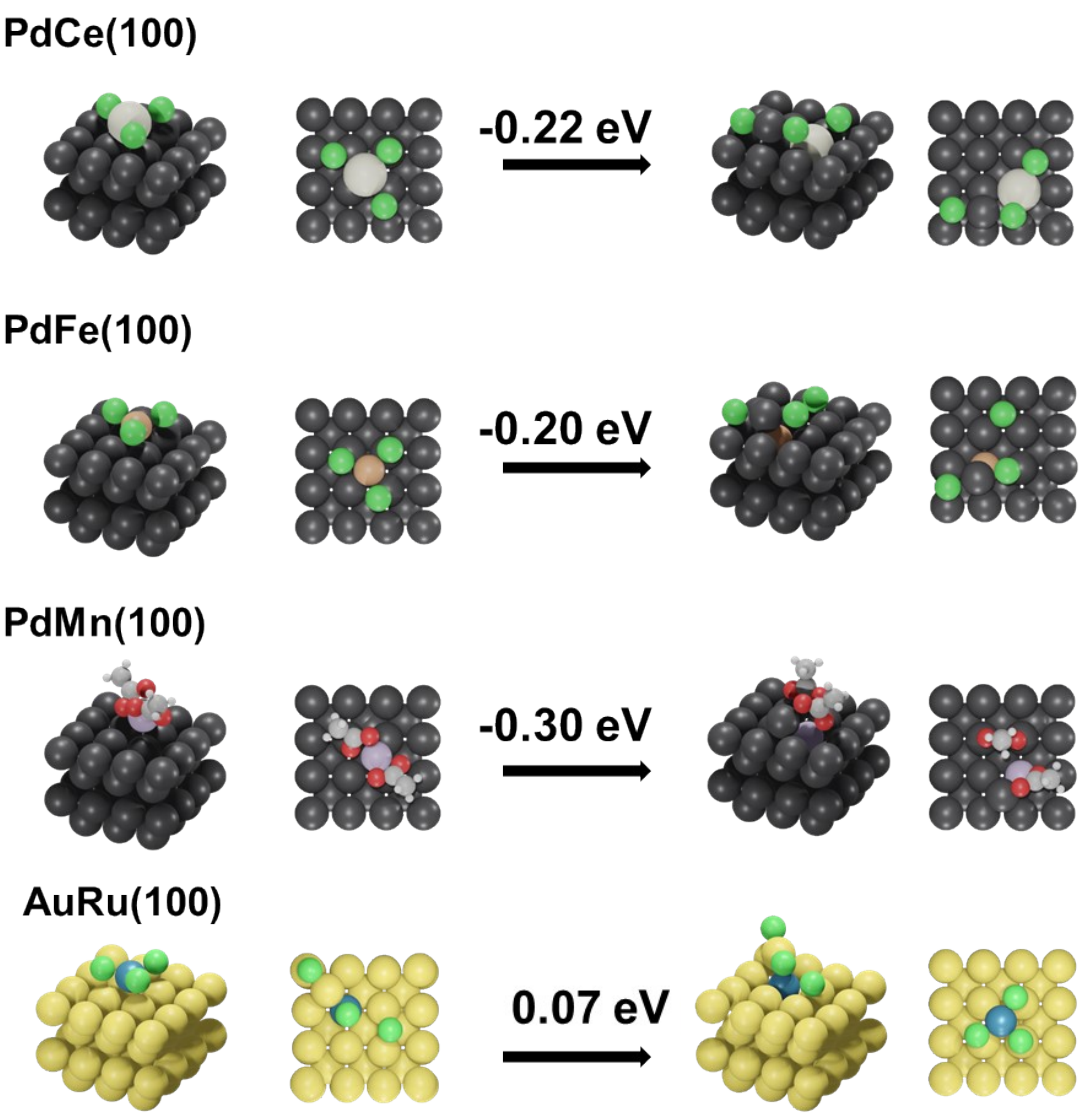

Fig. S8. Reaction energies of $CeCl_3$, $FeCl_3$ and $Mn(CH_3CO_2)_2$ exchange with Pd(100) and $RuCl_3$ exchange with Au(100). (Color code: Pd: dark gray, Ce: ivory, Fe: orange, Mn: purple, Cl: green, C: gray, H: white, O: red, Au: gold and Ru: blue)

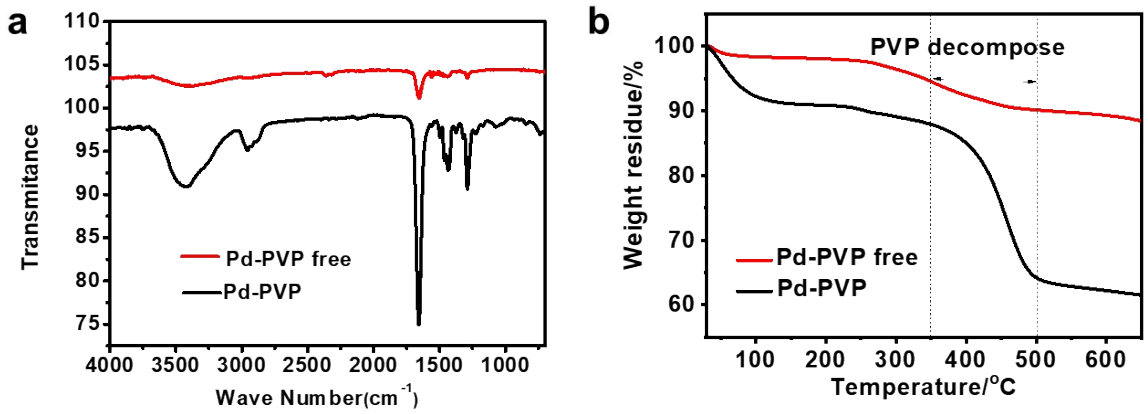

Fig. S9. Pd-PVP and Pd-PVP free fourier transform-infrared (FT-IR) spectra (a) and thermogravimetric thermal analysis (TGA) (b).

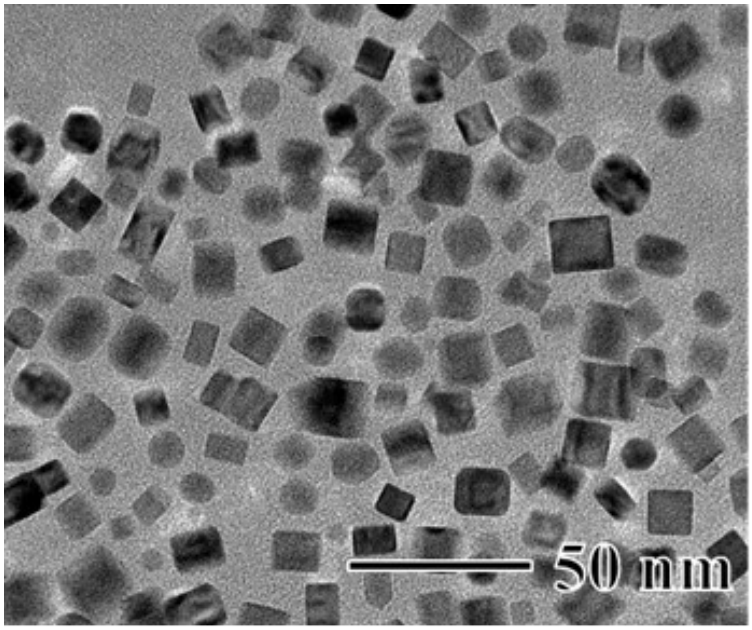

Fig. S10. TEM images of PVP-free Pd nanocubes.

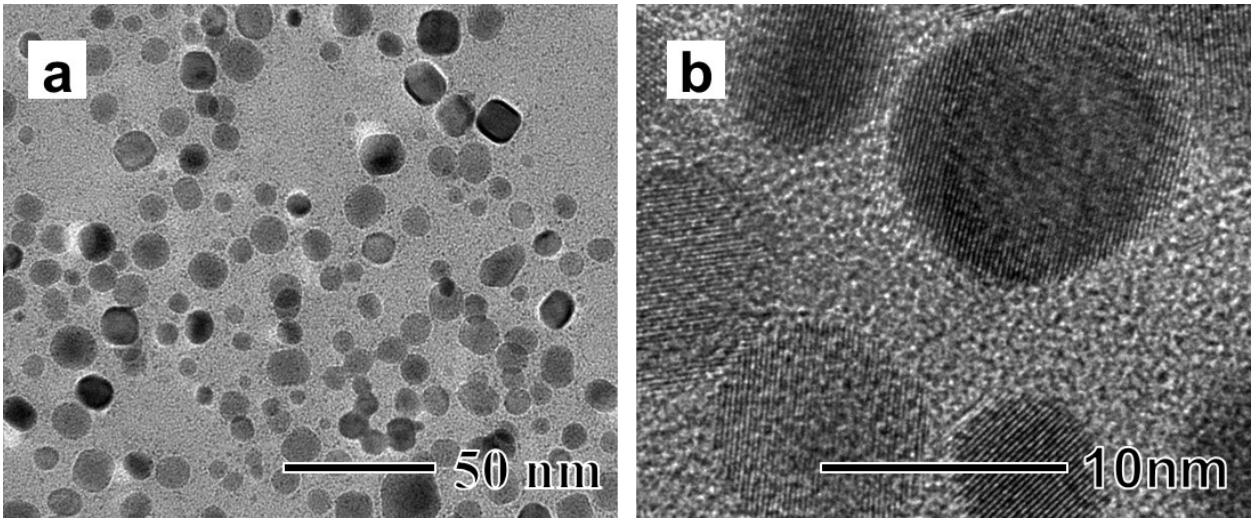

Fig. S11. TEM (a) and HRTEM(b) of $PdRu_{20}$-PVP free.

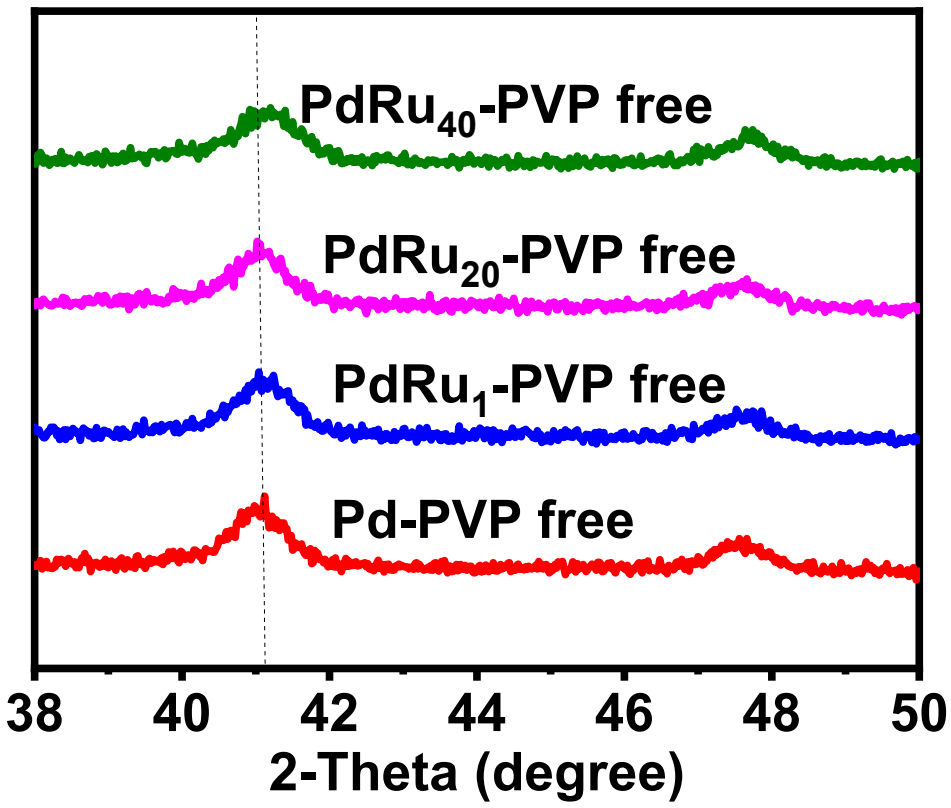

Fig. S12. XRD patterns of PVP-free Pd and PdRu nanocubes with difference Ru ratio.

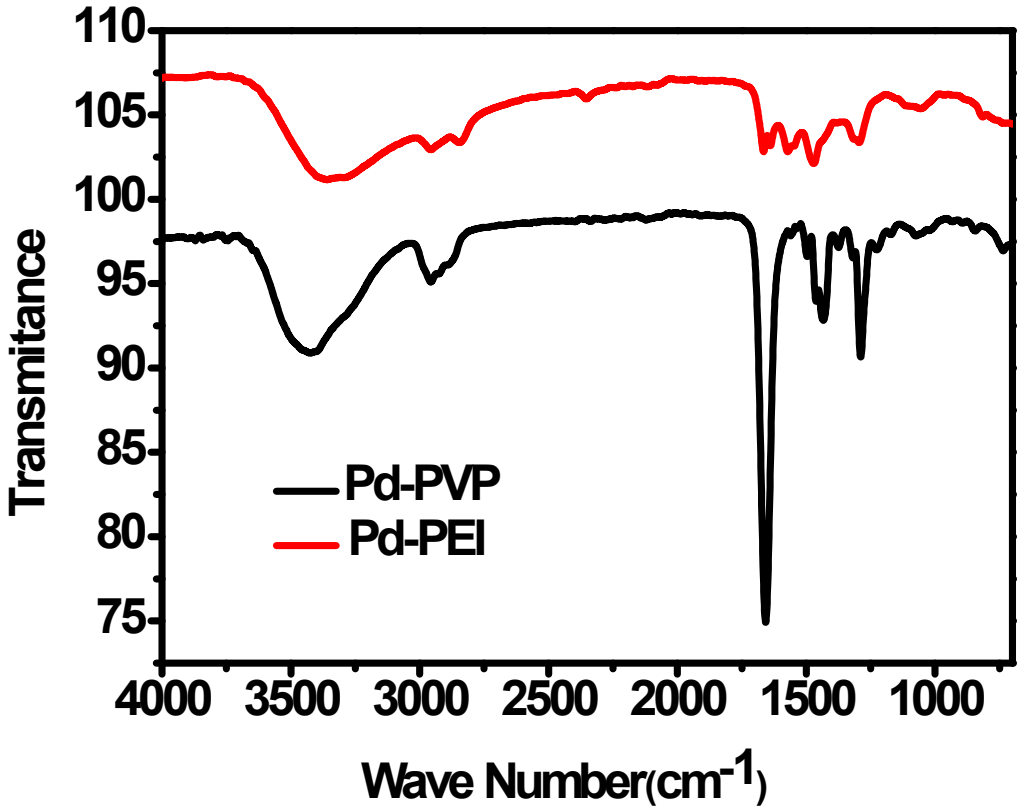

Fig. S13. Pd-PVP and Pd-PEI Fourier transform-infrared (FT-IR) spectra.

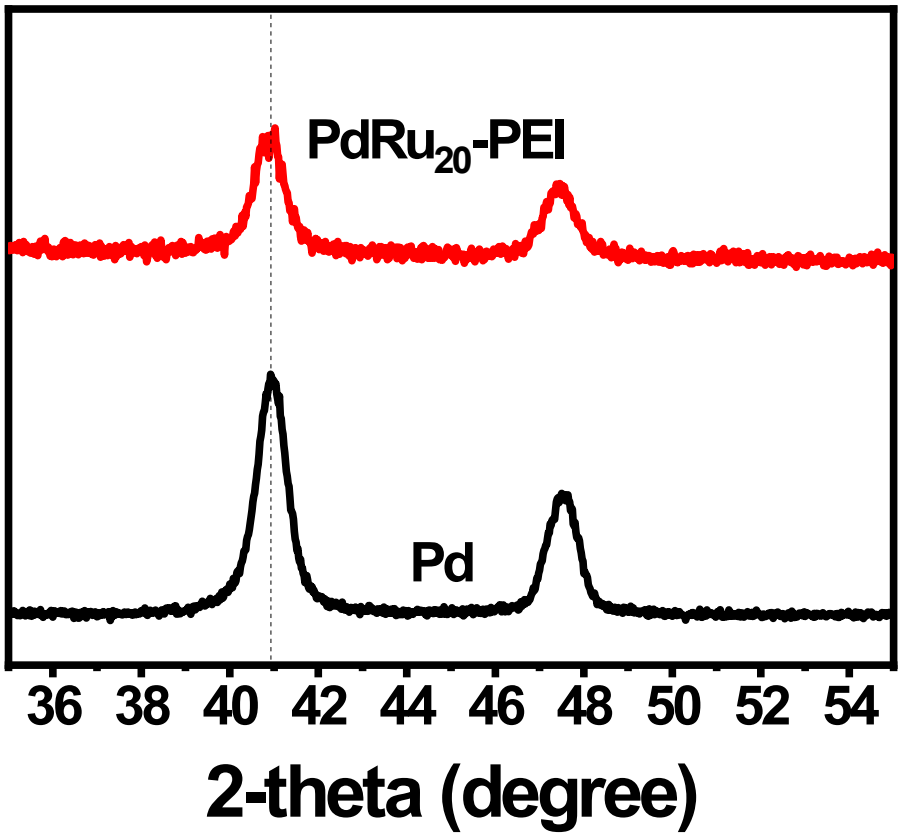

Fig. S14. XRD patterns of $PdRu_{20}$ nanocubes prepared with difference pH value.

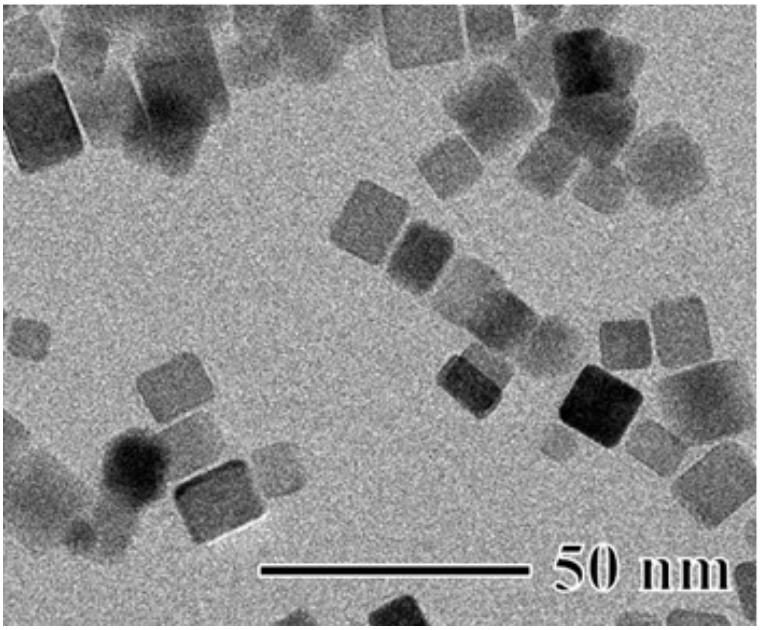

Fig. S15. TEM images of PEI-stabilized Pd nanocubes.

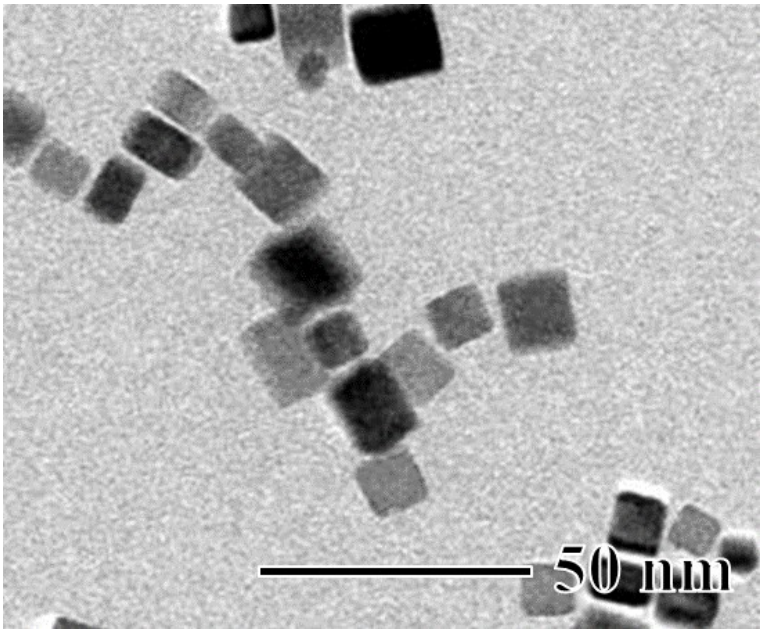

Fig. S16. TEM images of PEI-stabilized $PdRu_{20}$ nanocubes.

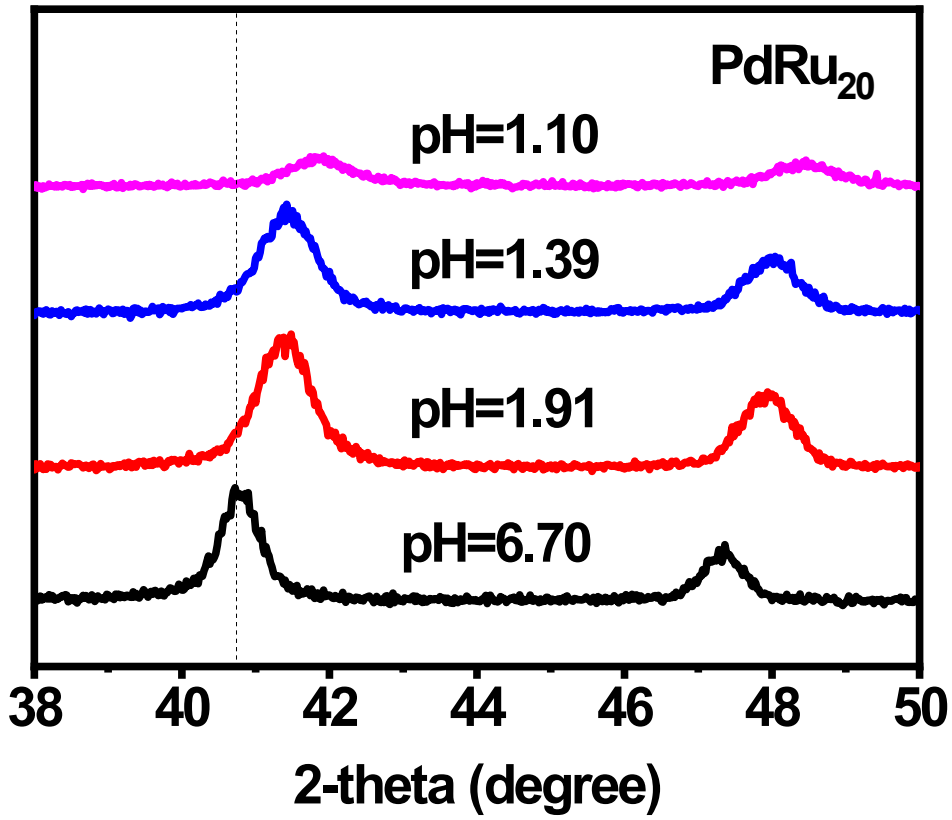

Fig. S17. XRD patterns of $PdRu_{20}$ nanocubes prepared with difference pH value.

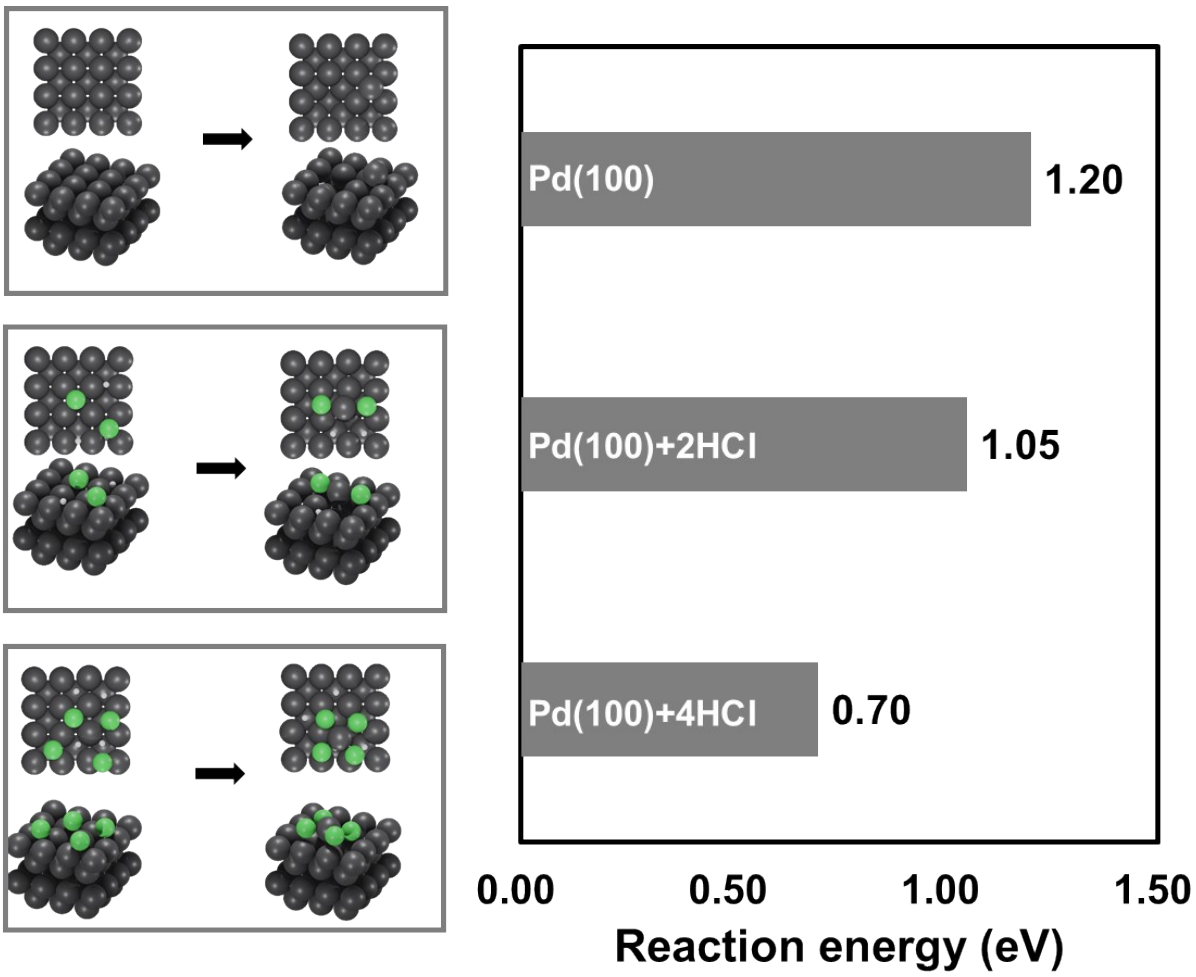

Fig. S18. Pd defect formation energies in the presence of HCl. (Color code: Pd: dark gray and Cl: green)

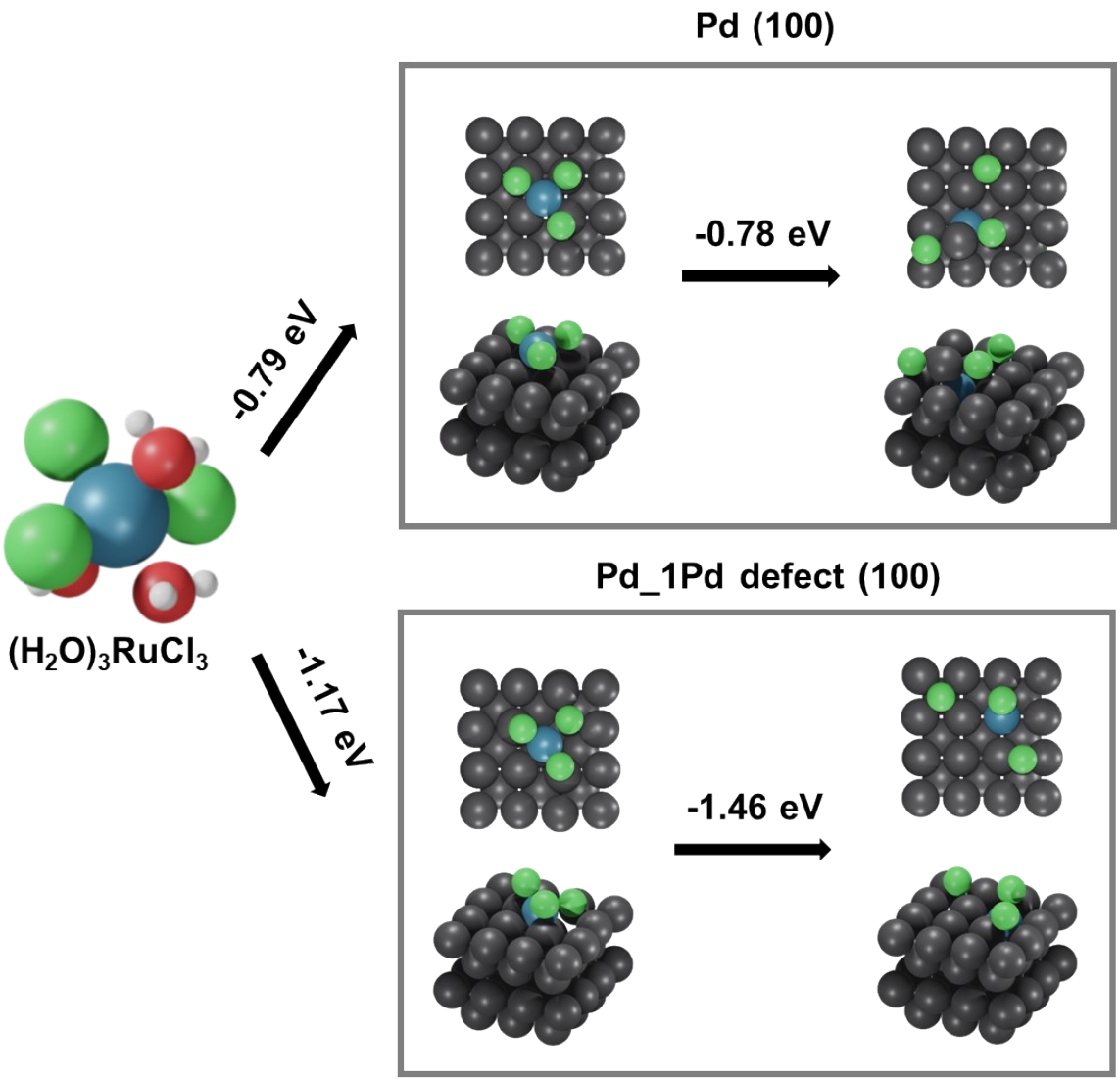

Fig. S19. Reaction energies of $RuCl_3$ exchange with pristine Pd(100) and with one-Pd-atom-defected-Pd(100) surfaces. (Color code: Pd: dark gray, O: red, H: white, Cl: green and Ru: blue)

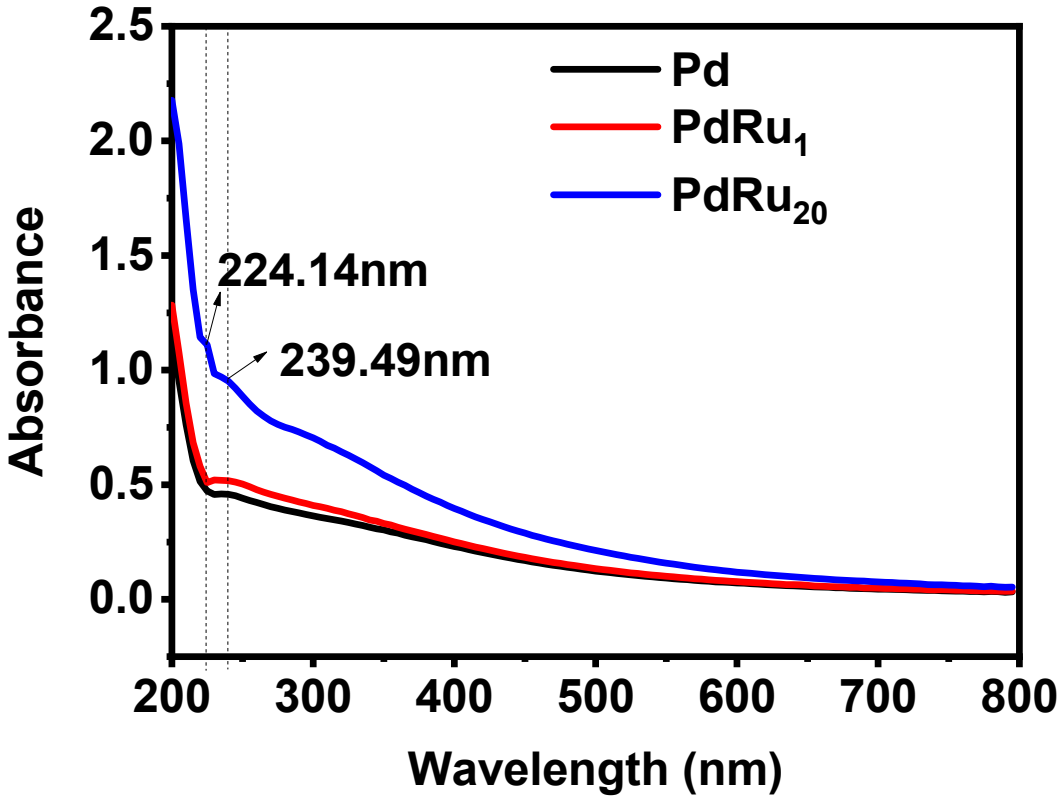

Fig. S20. The UV-vis pattern of Pd, PdRu suspension. From this UV-vis figure, the H_2PdCl_4 (two peaks at 224.14nm and 239.49nm) was found in the supernatant of $PdRu_{20}$ solution.

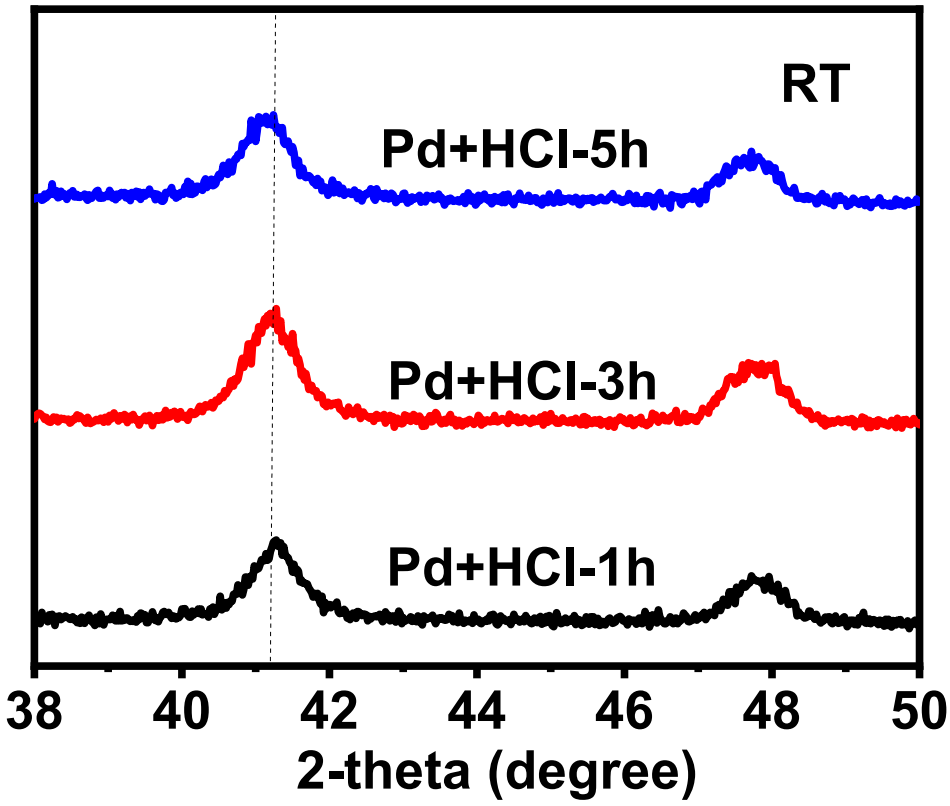

Fig.S21. XRD patterns of Pd + HCl without Ru.

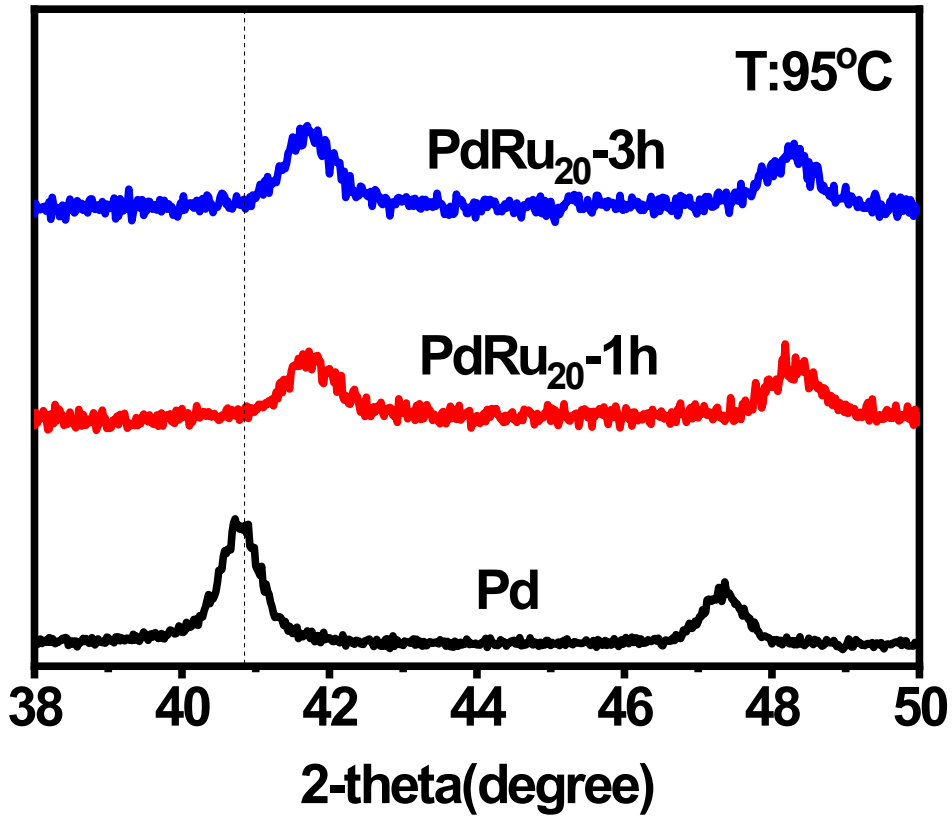

Fig. S22. XRD patterns of $PdRu_{20}$ at 95°C with difference reaction time.

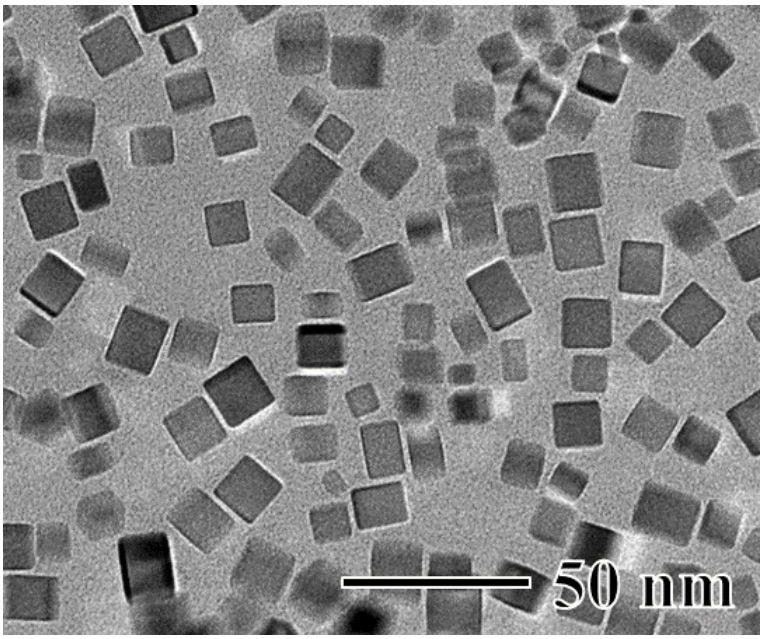

Fig. S23. TEM images of $PdRu_{20}$ at 95°C.

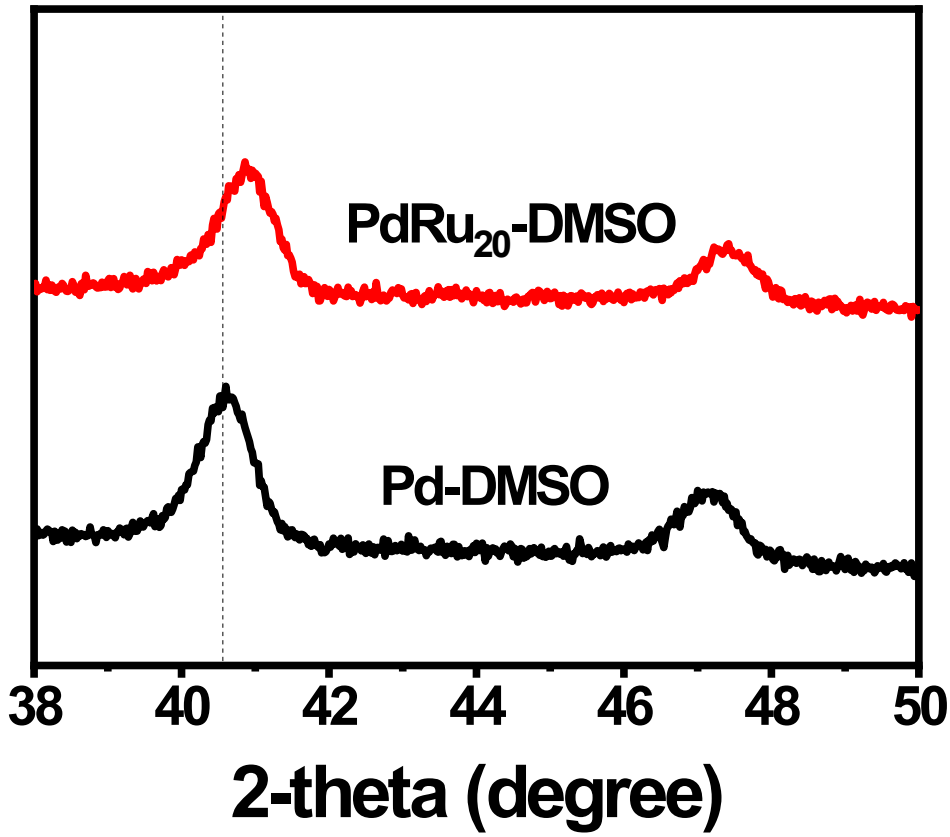

Fig. S24. XRD patterns of $PdRu_{20}$ in DMSO.

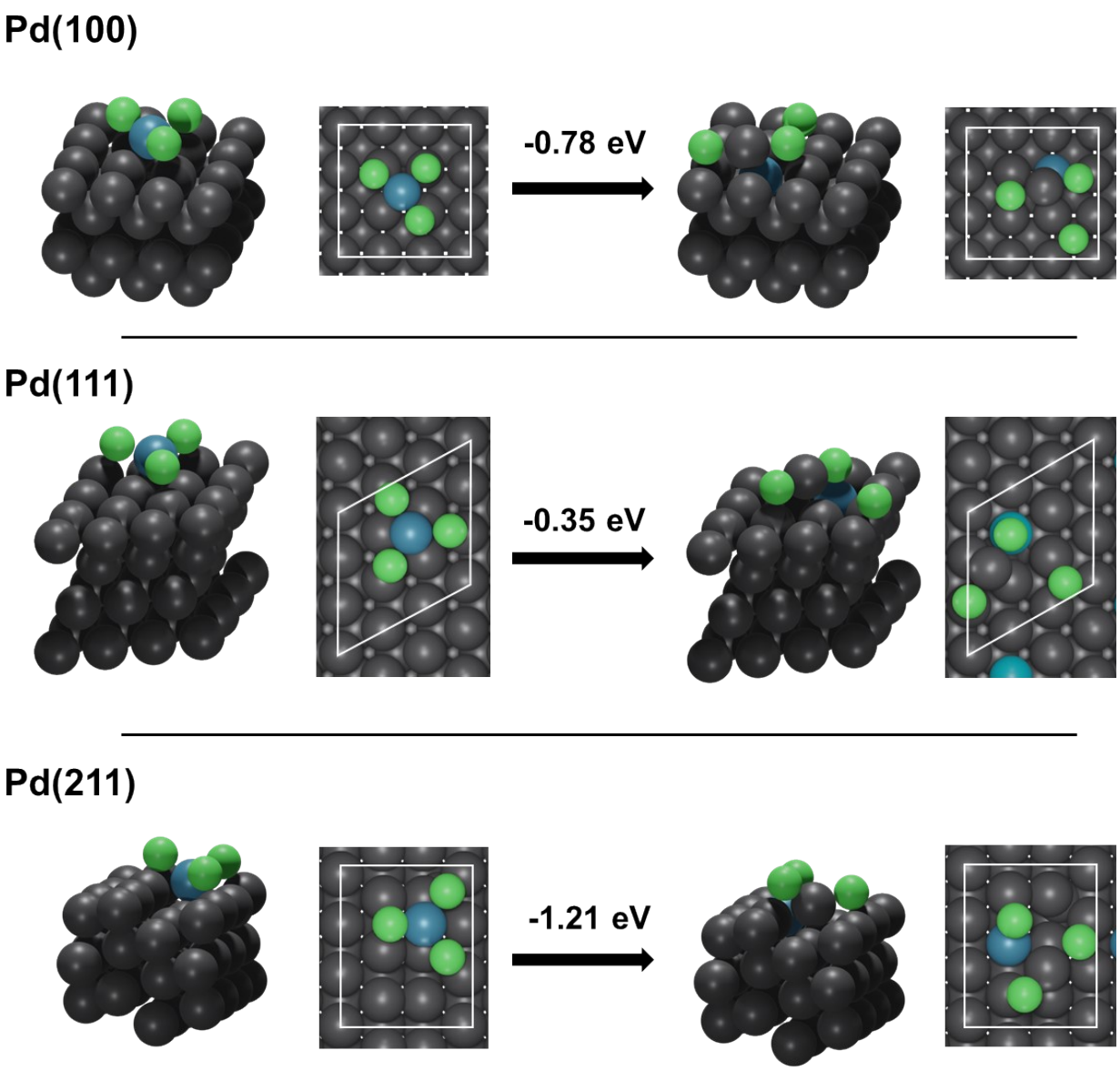

Fig. S25. Reaction energies for $RuCl_3$ exchange with Pd(100), Pd(111) and Pd(211) surface. (Color code: Pd: dark gray, Cl: green and Ru: blue)

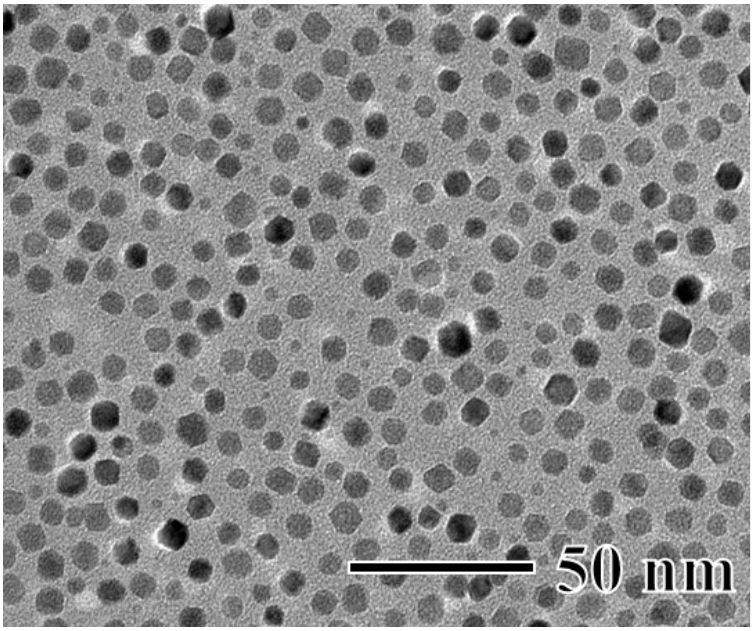

Fig. S26. The images of Pd-sphere.

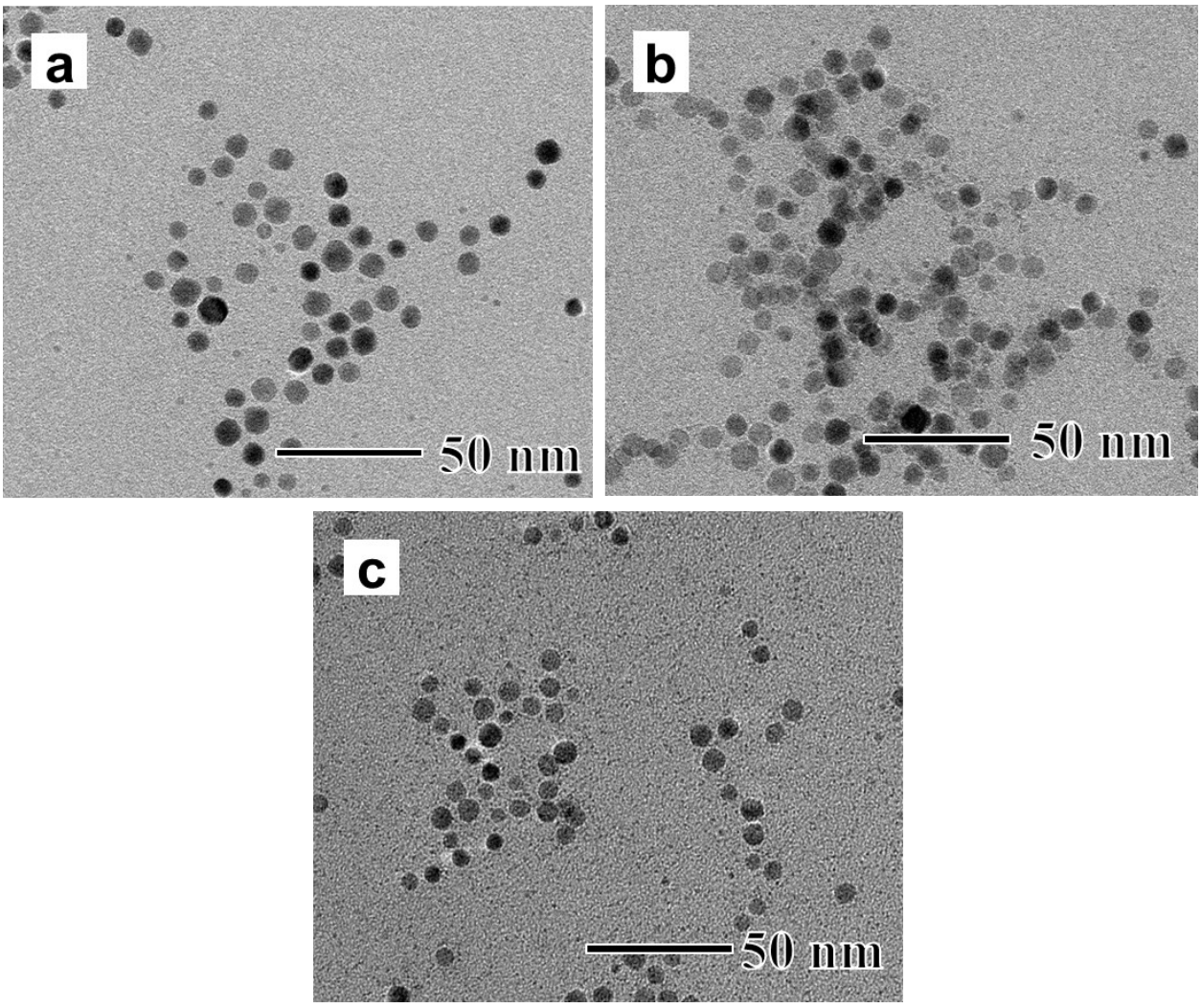

Fig. S27. The images of spherical $PdRu_1$(a), $PdRu_{20}$(b) and $PdRu_{40}$(c).

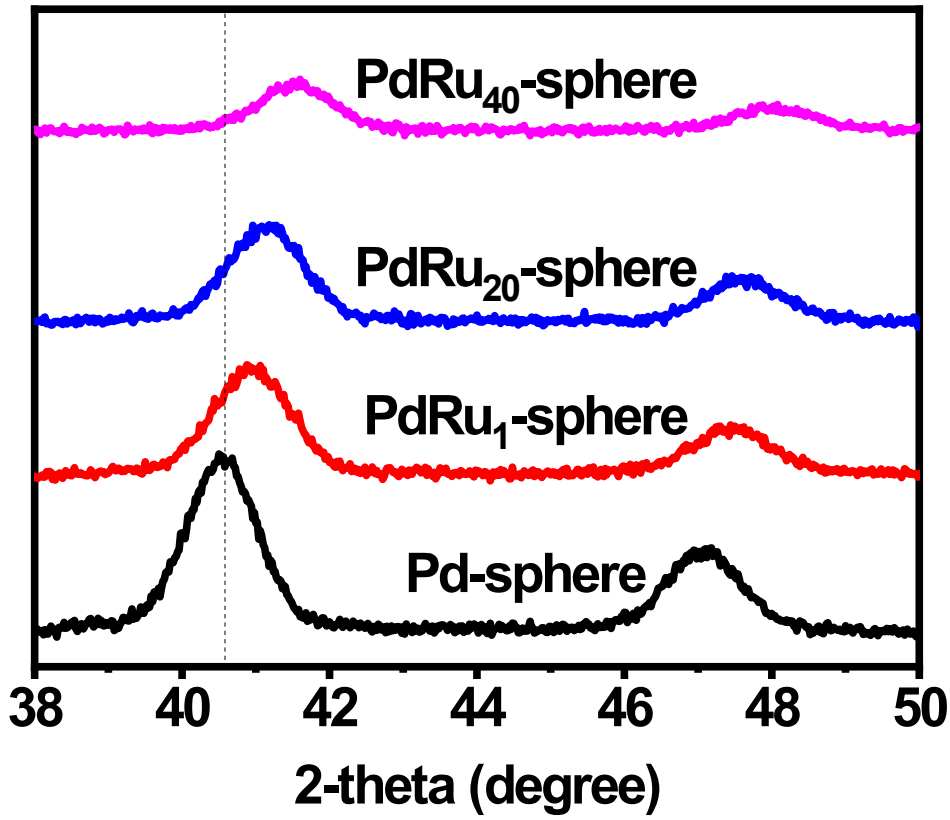

Fig. S28. XRD patterns of spherical PdRu nanoparticles.

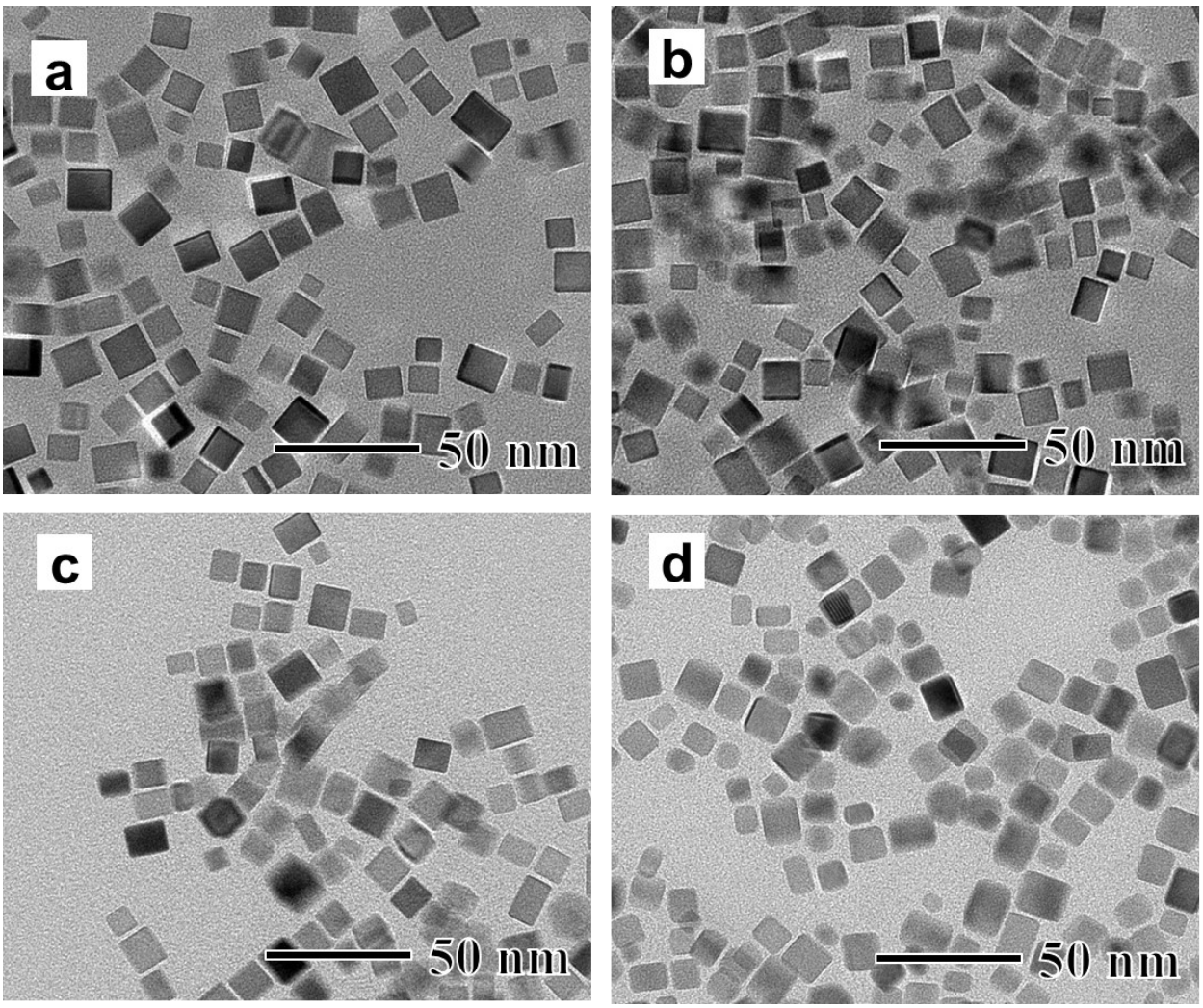

Fig. S29. The TEM images of PdCe (a), PdEu (b) PdMn (c) and PdFe (d).

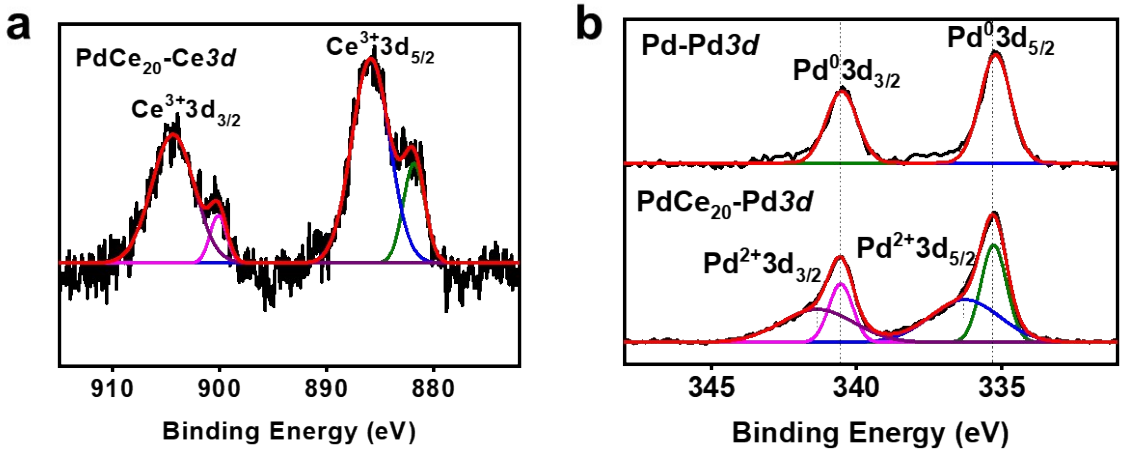

Fig. S30. The Ce3d and Pd3d XPS pattern of $PdCe_{20.}$ There are some Pd^{2+} leaving on Pd after the Ce^{3+} replaced, this phenomenon also found in PdRu.

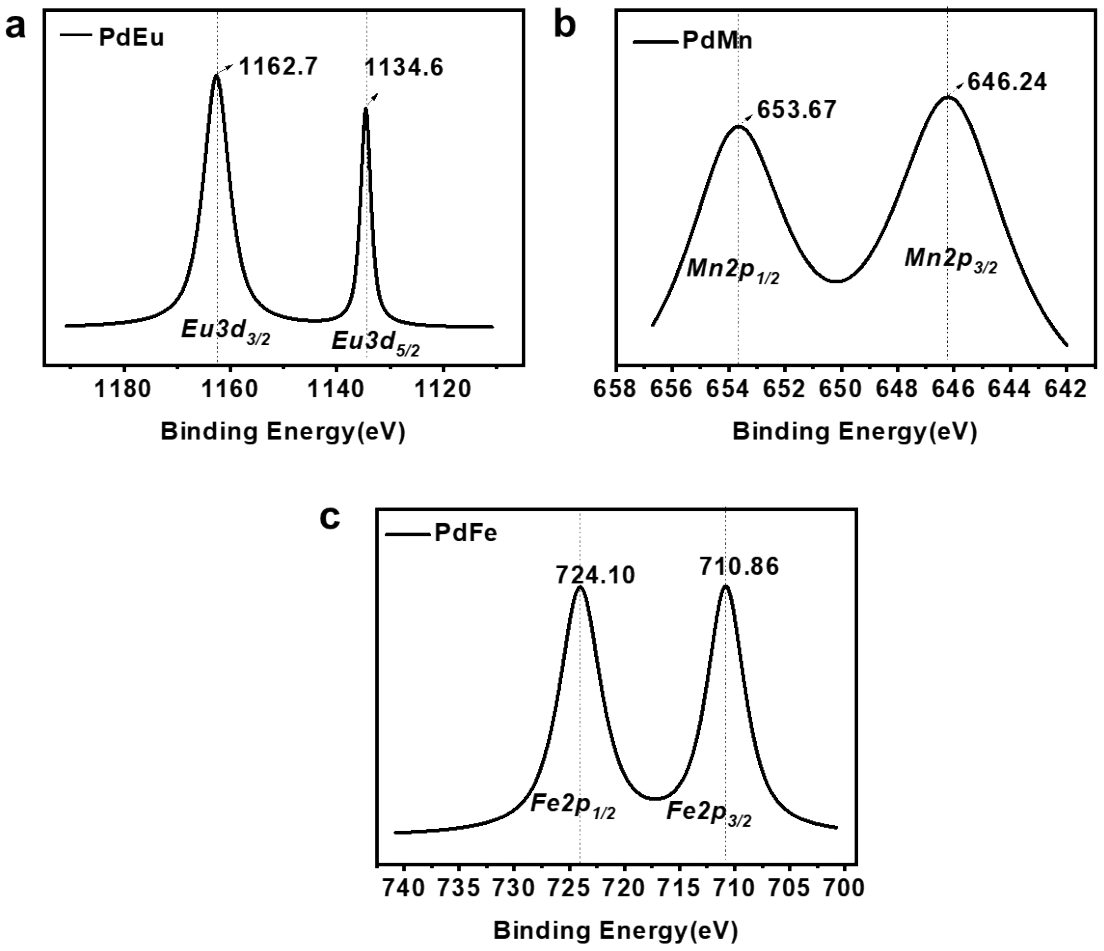

Fig. S31. The XPS spectrum of $PdEu_{20}$ (a), $PdMn_{20}$ (b), $PdFe_{20}$ (c).

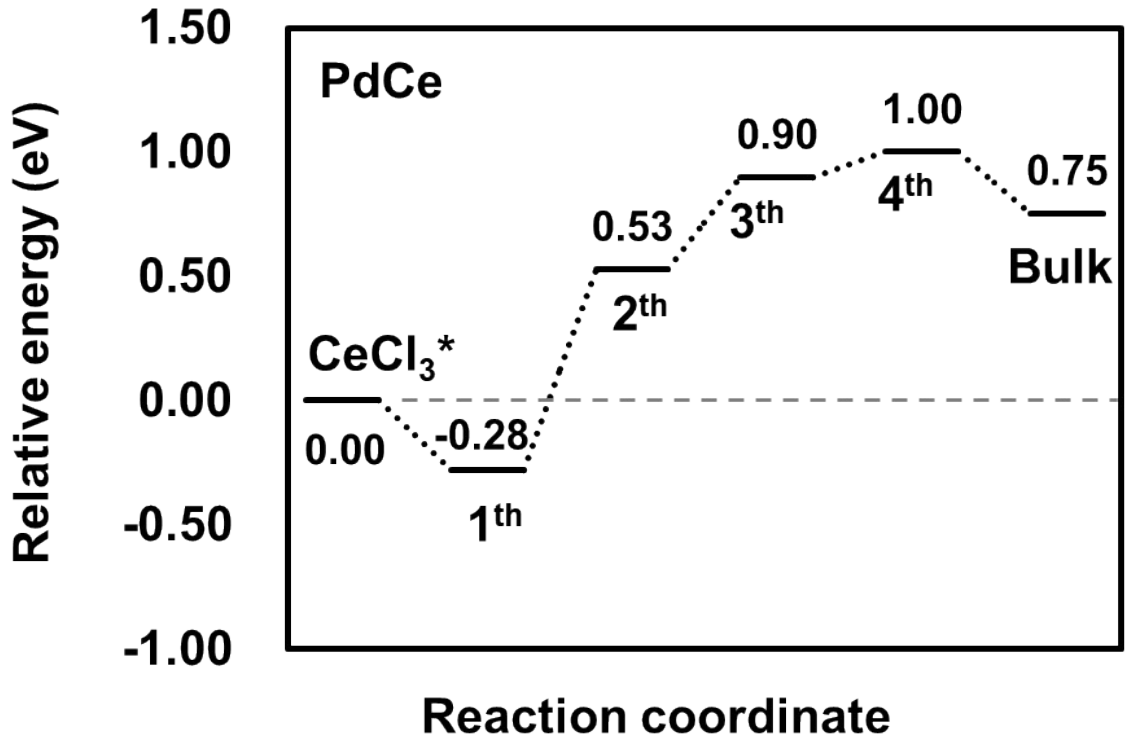

Fig. S32. Relative energy diagram of $CeCl_3$ exchange on Pd (100) surface. The dashed grey line denotes the energy of $CeCl_3$ adsorption on Pd (100).

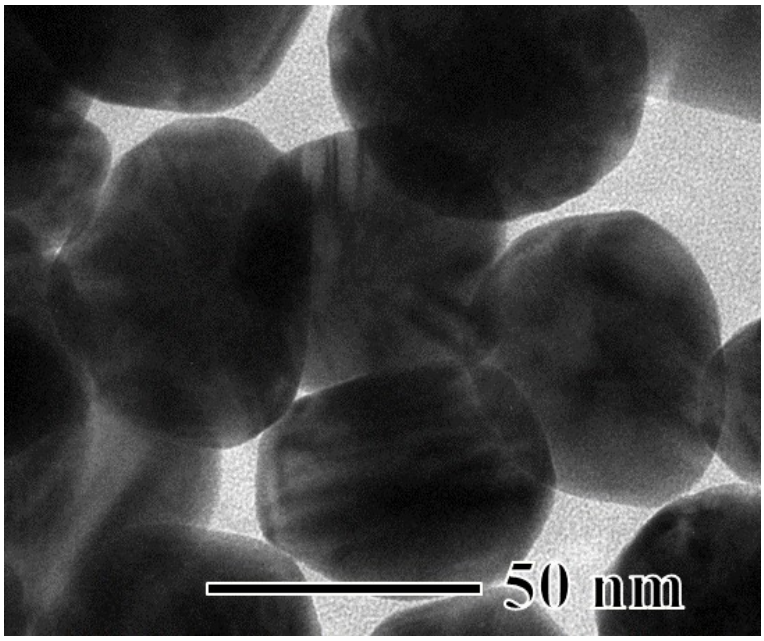

Fig. S33. The TEM images Au.

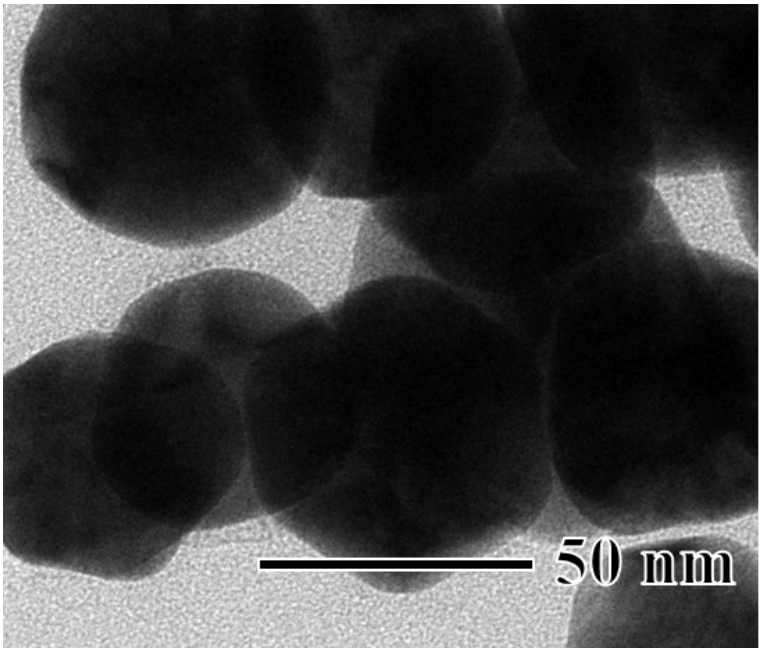

Fig. S34. The TEM images with different magnification of $AuRu_{20.}$

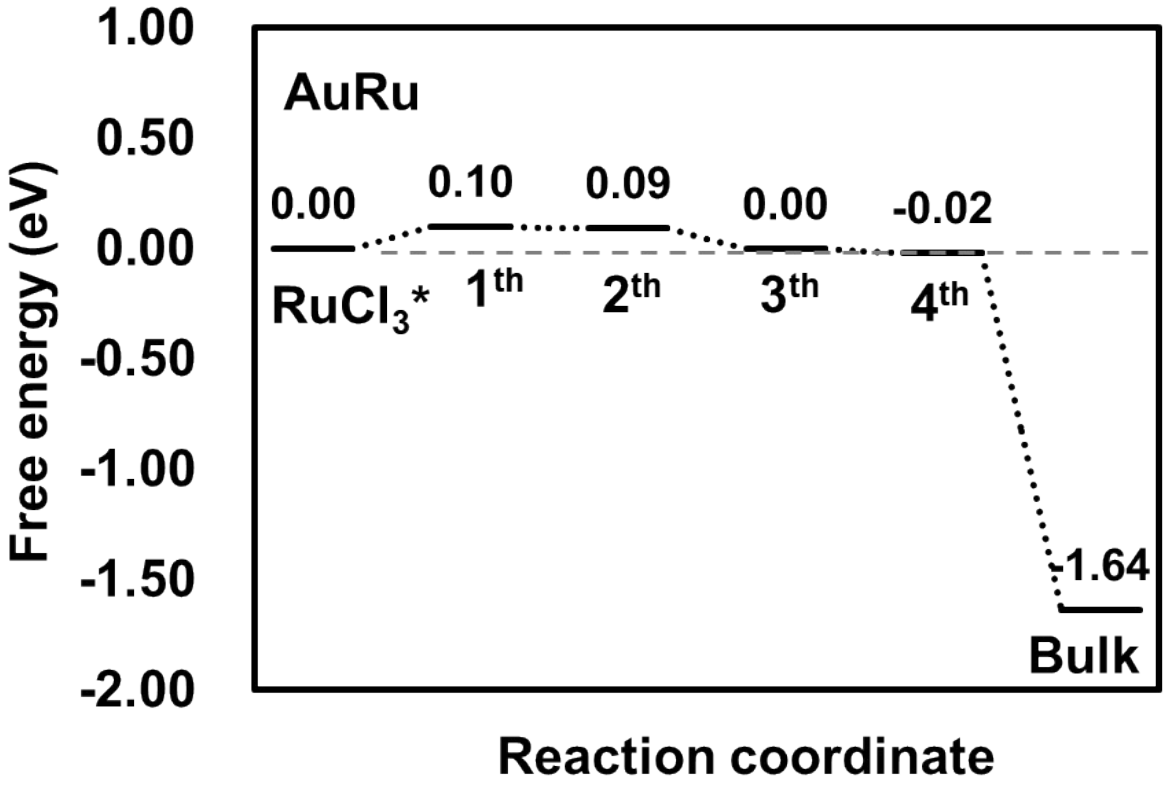

Fig. S35. Relative energy diagram of $RuCl_3$ exchange on Au (100) surface. The dashed grey line denotes the energy of $RuCl_3$ adsorption on Au (100).

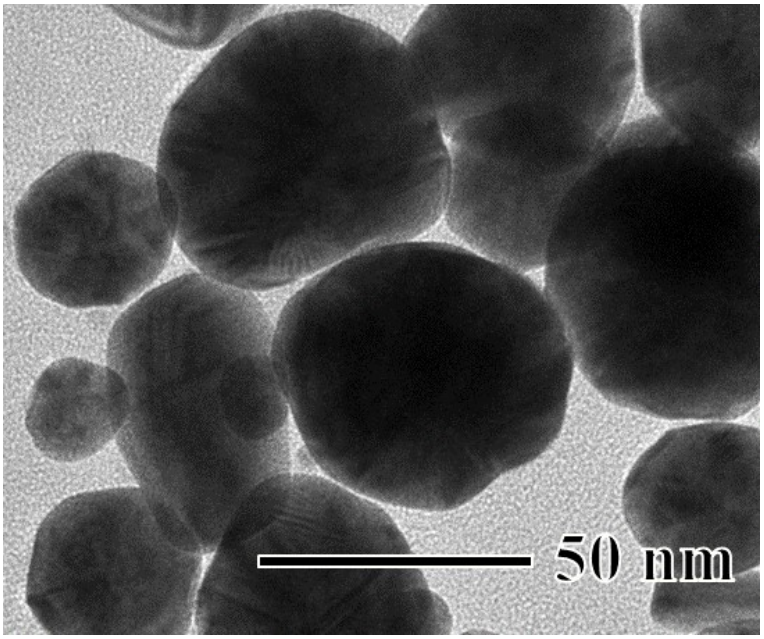

Fig. S36. The TEM images $AuEu_{20}$.

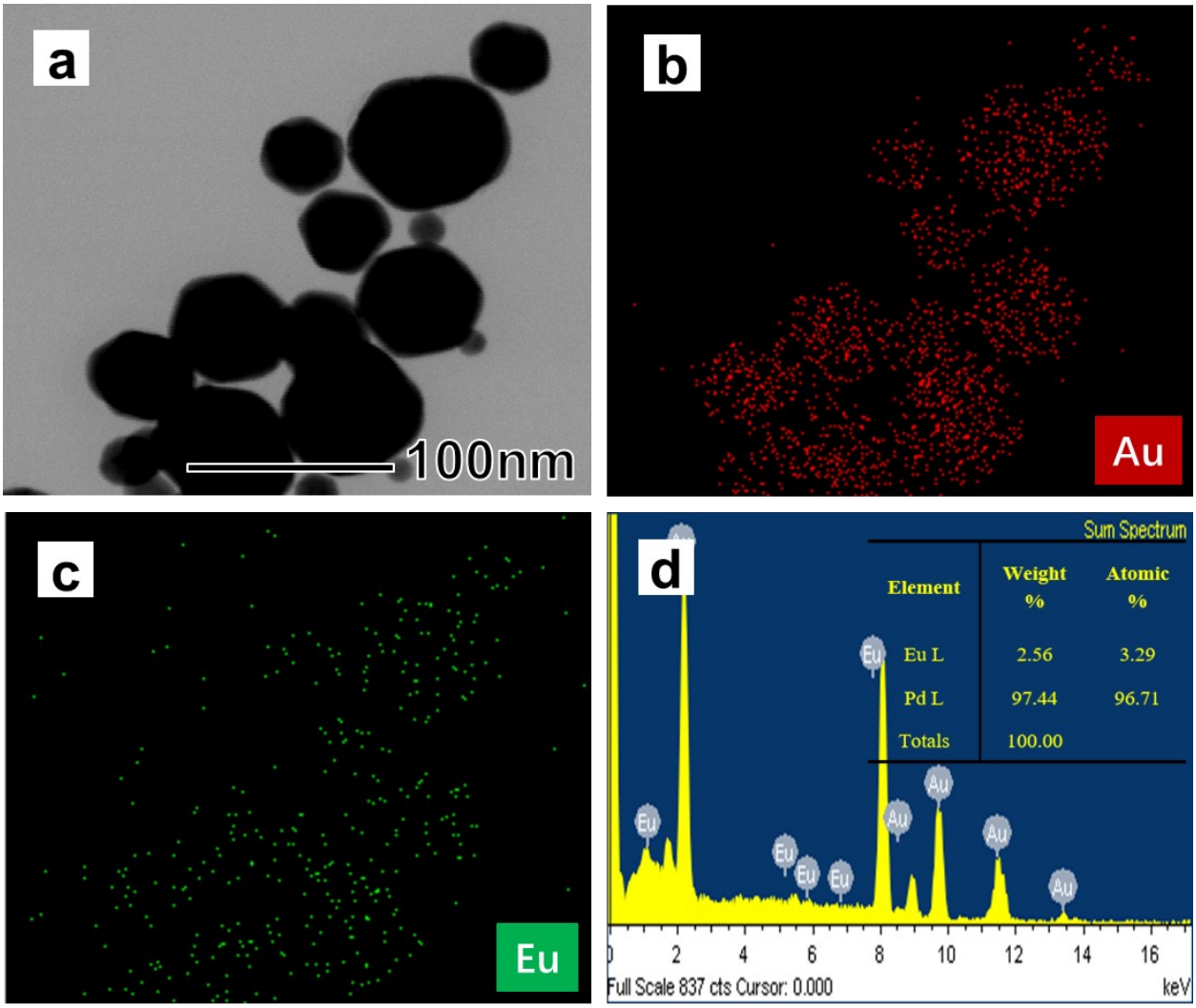

Fig. S37. The EDS mapping (**a,b,c**) and the EDX spectrum (**d**) of $AuEu_{20}$.

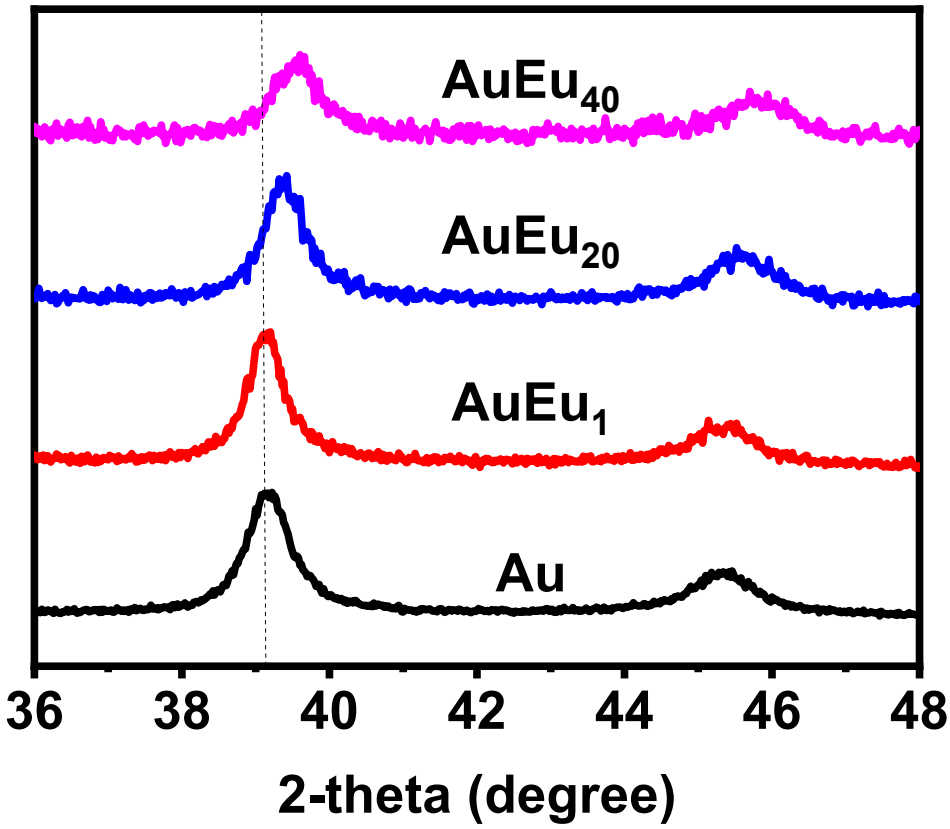

Fig. S38. XRD patterns of AuEu nanoparticles with difference Eu/Au ratio.

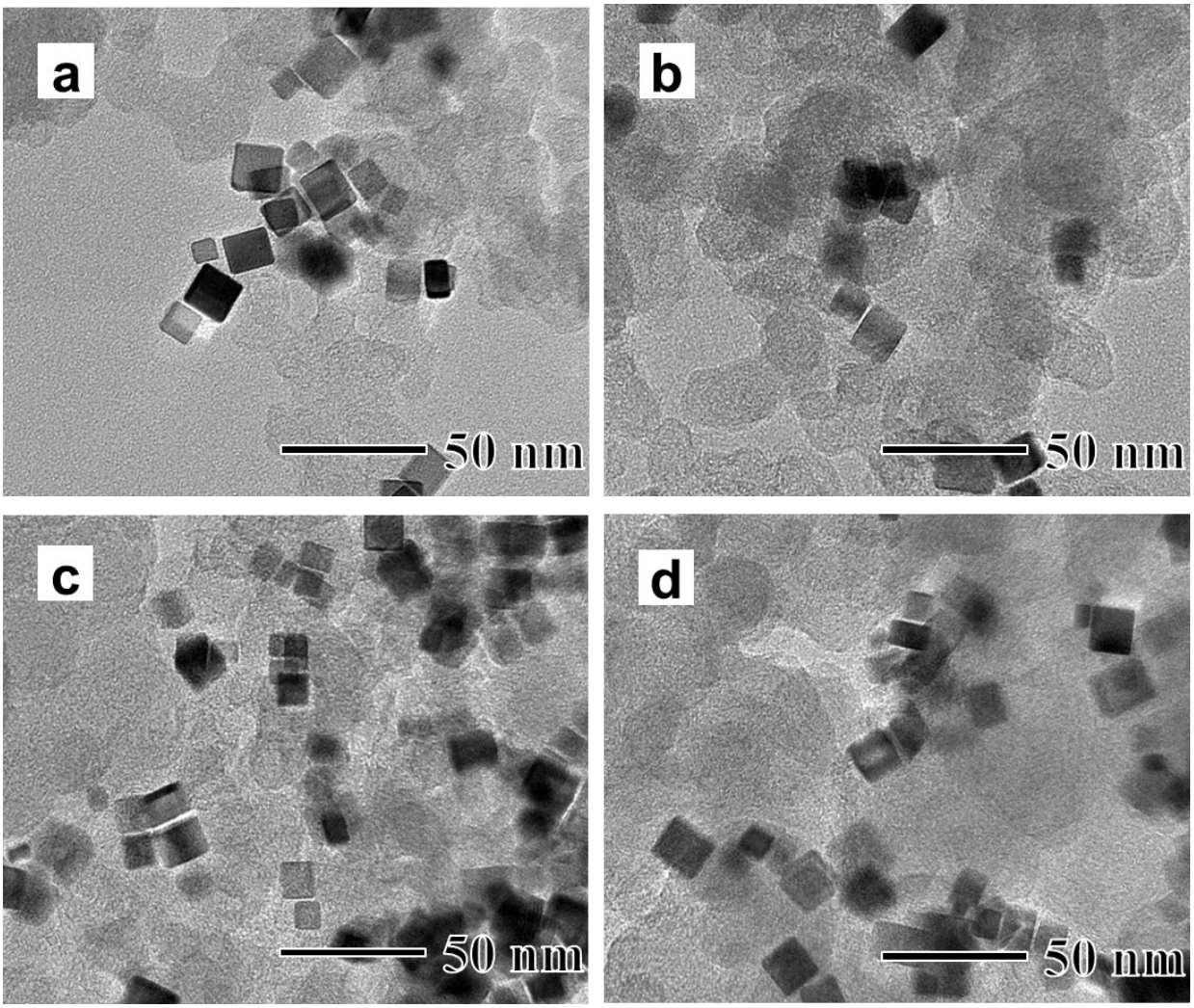

Fig. S39. The TEM images of Pd/C (a), $PdRu_1$/C (b), $PdRu_{20}$/C (c), and $PdRu_{40}$/C (d).

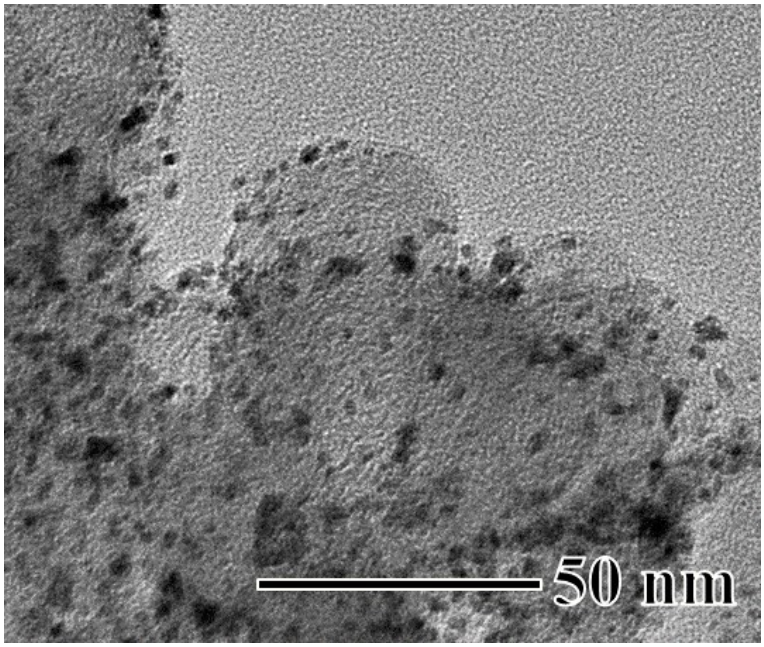

Fig. S40.TEM images of Pt/C nanoparticles.

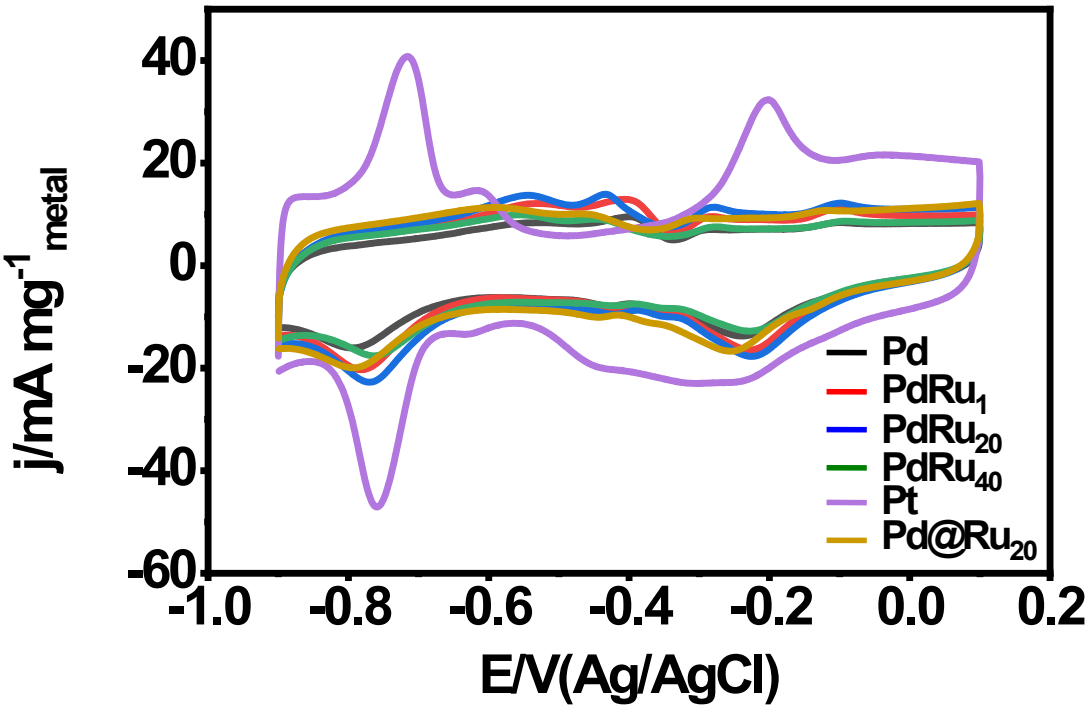

Fig. S41. CV curves of Pd/C, PdRu/C, Pd@Ru/C and commercial Pt/C. The electrochemical surface areas (ECSA) were estimated by the reduction region of PdO to Pd and PtO to Pt between -0.9 and 0.1 V. For Pd oxide reduction, the oxide reduction peak of PdO at around -0.23 V vs Ag/AgCl in 1M KOH.

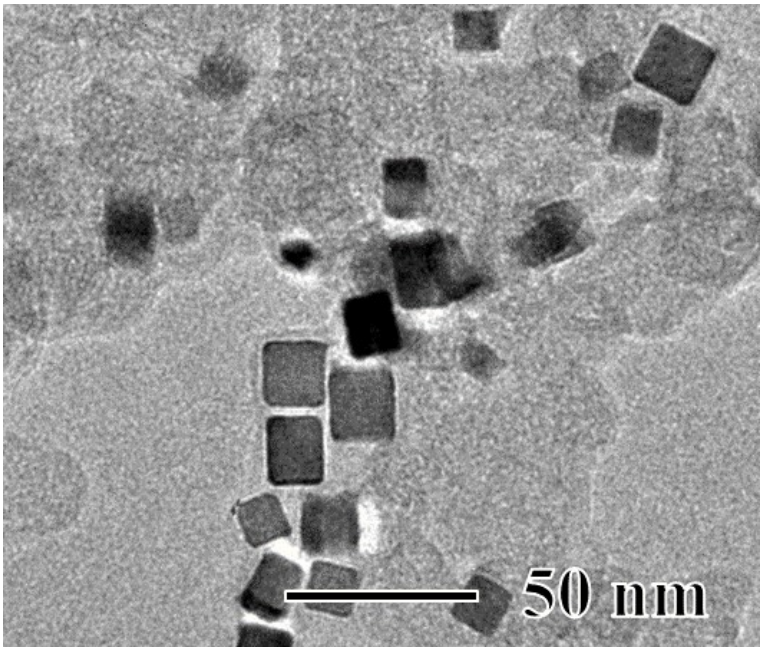

Fig. S42. TEM images of Pd@Ru_{20}/C nanoparticles.

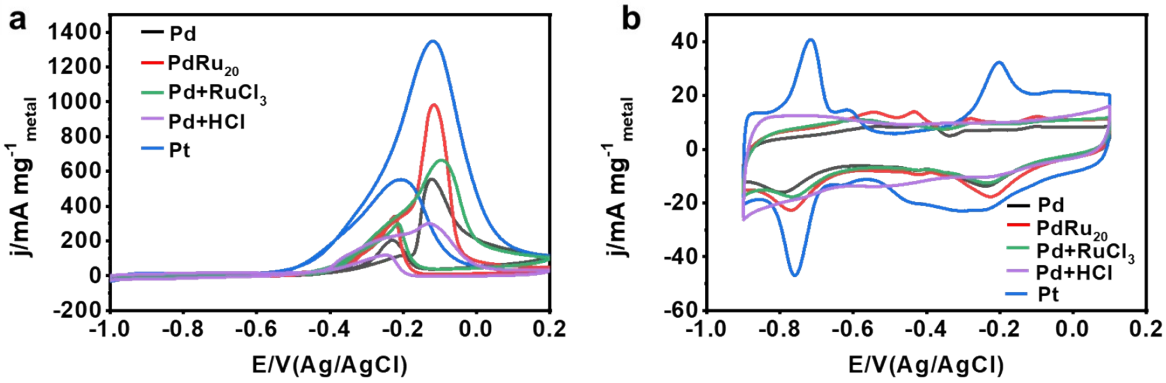

Fig. S43. (a), Cyclic voltammetry (CV) curves of catalysts in 1 M CH_3OH + 1 M KOH electrolyte. The scan rate was 50 mV s^{-1}, and the current density was based on the loading amount of PdRu. (b), the corresponding ECSA. In the absence of $RuCl_3$, the MOR performance of Pd+HCl decreased significantly. In the absence of hydrochloric acid, the MOR properties of Pd+$RuCl_3$ and Pd are basically the same. Those results indicated the Ru cation increased the MOR activity.

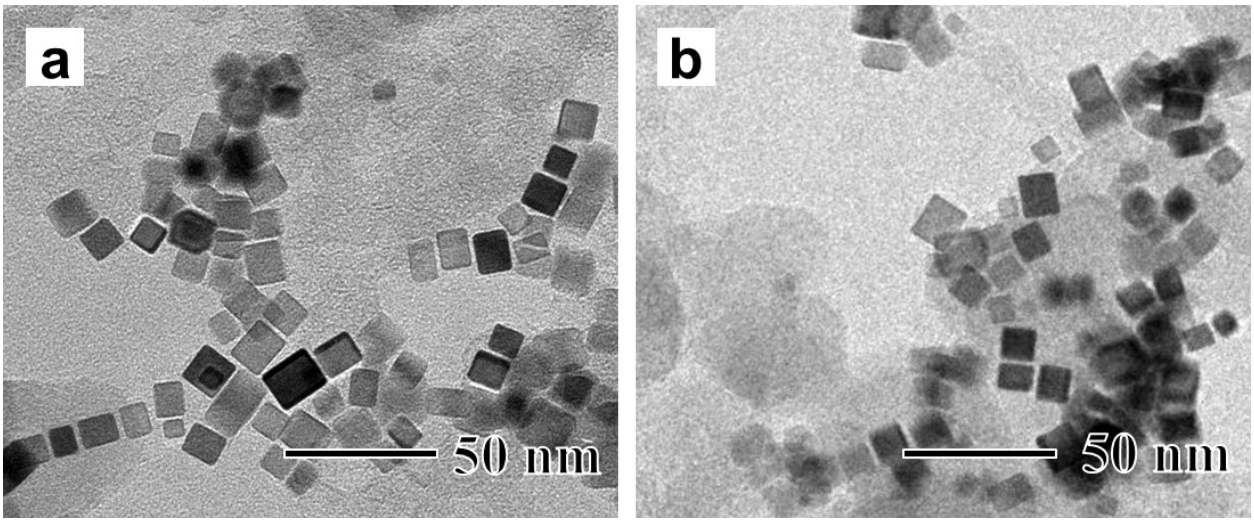

Fig. S44. The TEM images of PdCe/C (a), PdEu/C (b).

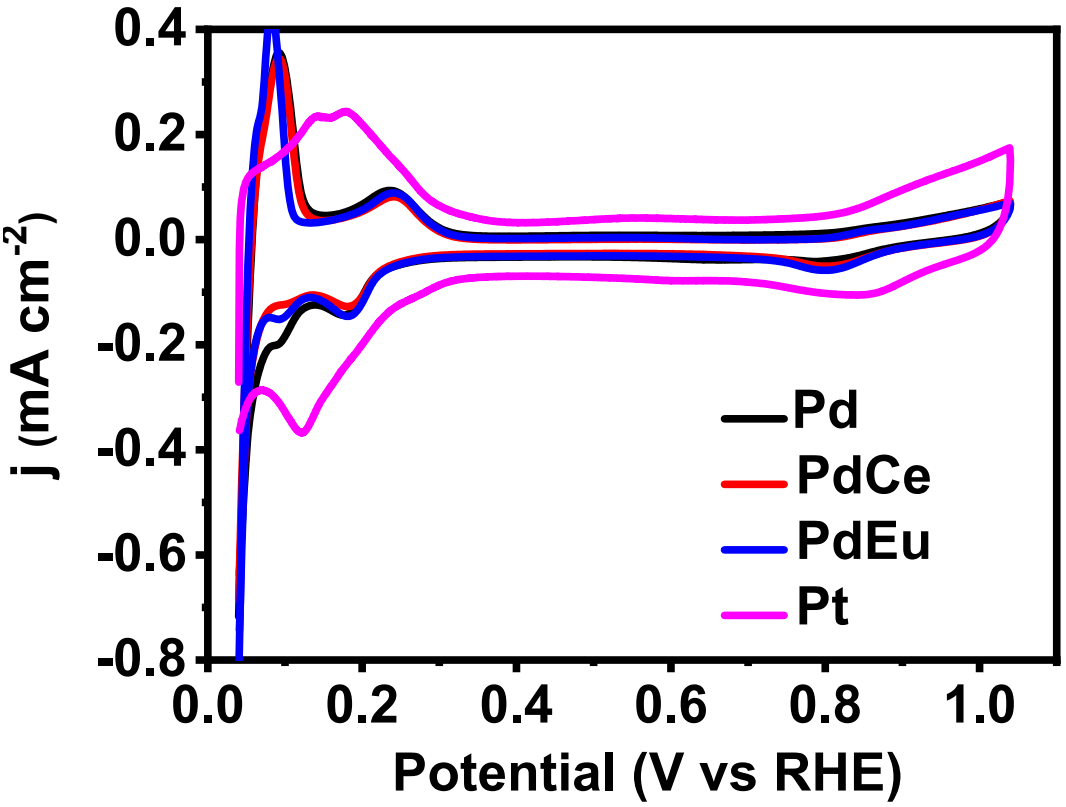

Fig. 45. CV curves of Pd/C, PdCe/C, PdEu/C, and commercial Pt/C. Cyclic voltammetry (CV) measurements were scanned from 0.05V-1.05V. The electrochemical surface areas (ECSA) of HER were determined by the Pd-O reduction also. The Pd and Pt oxide reduction peak located about 0.75 V was used for ECSA calculation in 0.5 M H_2SO_4 solution.

Table S1. ICP data of PdRu with controlling Ru concentration.

Catalysts	Molar fraction of metal (%)				
	Pd	Ru	(Ru+Pd)	Ru/Pd ratio	Ru cation exchanged ratio
$PdRu_1$	20.6	0.066	2.0666	0.33%	33.0%
$PdRu_{20}$	23	0.171	2.3171	0.78%	3.9%
$PdRu_{40}$	20.7	0.28	2.098	1.42%	3.6%
$PdRu_{60}$	7.64	0.087	0.7727	1.20%	2.0%
$PdRu_{100}$	21.3	0.208	2.1508	1.03%	1.0%

Table S2. ICP data of Pd@Ru with controlling Ru concentration.

Name	Molar fraction of metal (%)			
	Pd	Ru	(Ru+Pd)	Ru/Pd ratio
$Pd@Ru_{1}$	17.2	0.47	1.767	2.88%
$Pd@Ru_{20}$	18	1.22	1.922	7.14%
$Pd@Ru_{40}$	17.6	2	1.96	11.96%

Table S3. Zeta potential values of Pd-PVP nanocubes and Pd-PVP free nanocubes.

Name	Zeta Potential (mV) at pH=1.39			
	1th	2th	3th	Mean(1th-3th)
Pd-PVP	-12.9	-13.5	-15	-13.8
Pd-PVP free	-6.17	-6.76	-6.36	-6.43

Table S4. Zeta potential values of PEI-stabilized Pd nanocubes.

Name	Zeta Potential (mV) at pH=1.39			
	1th	2th	3th	Mean(1th-3th)
Pd-PVP	-12.9	-13.5	-15	-13.8
Pd-PEI	32.9	31.7	32.4	32.33

Table S5. Pd mass in solvent before and after HCl treatment, and Pd mass in solvent after Ru^{3+} cation exchanged.

Name	Molar fraction of metal (%)		
	Pd in solvent（ug）	**Pd in bulk（mg）**	**Pd dissolved ratio**
Pd-before HCl treatment	11.556	17.8	0.063%
Pd-after HCl treatment	26.720	17.8	0.150%
$PdRu_{20}$	102.54	17.8	0.576%

Table S6. Elemental composition of PdM measured by ICP.

Pd@PdM(M=Fe,Mn,Ce,Eu)	Molar fraction of metal (%)			
	Pd	M	(M+Pd)	M/Pd ratio
$PdFe_{20}$	21.8	0.194	2.1994	1.69%
$PdMn_{20}$	12.2	0.013	1.2213	0.21%
$PdCe_{20}$	41.3	0.699	4.1999	1.29%
$PdEu_{20}$	42.8	1.05	4.385	1.72%

Table S7. ICP data of AuEu.

Name	Molar fraction of metal (%)			
	Au	Eu	(Eu+Au)	Eu/Au ratio
$AuEu_1$	28.3	0.199	2.8499	0.91%
$AuEu_{20}$	17.5	0.206	1.7706	1.77%
$AuEu_{40}$	20.5	0.564	2.1064	2.10%

Table S8. DFT-calculated free energy of the MOR intermediates on Pd(100) and PdRu(100).

MOR intermediates	Pd(100) (eV)	PdRu(100) (eV)
***CH_3OH**	-0.22	-0.42
***CH_2OH**	0.55	0.26
***CHOH**	0.28	-0.05
***COH**	-0.09	-0.16
***CHO**	0.03	0.47
***HCOOH**	-0.04	-0.30
***HCOO**	0.43	0.15
***CH_2O**	-0.04	-0.66
***CO**	-0.74	-1.01
***CH_3O**	0.76	0.18
***COOH**	0.40	0.13

Table S9. ECSAs of PdRu/C, Pd/C, Pt/C, and Pd@Ru_{20}/C.

Sample	ECSA (m^2/g_{metal})	ECSA of 7.84 ug metal (cm^2)
Pd	19.5476	1.5325
$PdRu_1$	22.3452	1.7519
$PdRu_{20}$	24.7024	1.9367
$PdRu_{40}$	19.9167	1.5615
Pt	56.5357	4.4324
Pd@Ru_{20}	17.1131	1.3416

Table S10. ECSAs of $PdEu_{20}$/C, $PdCe_{20}$/C, Pd/C, and Pt/C.

Sample	ECSA (m^2/g_{metal})	ECSA of 7.84 ug metal (cm^2)
Pd	12.5595	0.9847
$PdEu_{20}$	13.0952	1.0268
$PdCe_{20}$	11.2309	0.8805
Pt	26.1309	2.0487

Supplementary Note | Calculation details of relative energy diagram of PdRu exchange:

To construct the relative energy diagram of PdRu exchange reaction (Fig. 3b), we started from calculating $RuCl_3$ adsorption energy ($E_{RuCl_3, ads}$) using isolated $RuCl_3 \cdot (H_2O)_3$ as a reference state as follows:

$$E_{RuCl_3, ads} = E_{RuCl_3/Pd, slab} - E_{Pd, slab} - E_{RuCl_3, gas},$$

where $E_{RuCl_3/Pd, slab}$ is the total energy of the $RuCl_3$ adsorbed slab, $E_{Pd, slab}$ is the total energy of the Pd pristine slab, and $E_{RuCl_3, gas}$ is the isolated $RuCl_3 \cdot (H_2O)_3$ energy deducted by the energy of three isolated H_2O molecules. Then, the energy required for adsorbed Ru to exchange with one Pd atom in Pd-nth-layer ($\Delta E_{relative, nth}$) is calculated as follows:

$$\Delta E_{relative, nth} = E_{RuCl_3@Pd\text{-}nth\text{-}layer, slab} - E_{Pd, slab} - E_{RuCl_3, gas}$$

where $E_{RuCl_3@Pd\text{-}nth\text{-}layer, slab}$ is the total energy of the $RuCl_3$ exchanged slab where Ru atom present in Pd-nth-layer (n=1~4). Here, the symbol '@' implies that $RuCl_3$ is exchanged with Pd while '/' represents that $RuCl_3$ is adsorbed. The optimized structures of Ru@Pd-nth-layer slab models are presented in Fig. 3d, denoted as '1^{st}', '2^{nd}', '3^{rd}' and '4^{th}', respectively. When Ru is located in Pd layers deeper than 4th-layer, we assumed that Ru is in the bulk region of Pd, and thus $\Delta E_{relative, bulk}$ is calculated using bulk alloy energy as follows:

$$\Delta E_{relative, bulk} = \{E_{PdCl_3/Pd, slab} + E_{Pd_{31}Ru_1, bulk}\} - \{E_{Pd, slab} + E_{Pd_{32}, bulk}\} - E_{RuCl_3, gas}$$

where $E_{PdCl_3/Pd,\ slab}$ is the total energy of Pd slab with chlorinated Pd adsorbed on the surface, which is constructed based on $RuCl_3$@Pd-4th-layer slab model and the Ru atom is substituted with Pd atom (see Fig. 3b for the optimized $E_{PdCl_3/Pd,\ slab}$, which is denoted as 'Bulk'). $E_{Pd_{31}Ru_1,\ bulk}$ is the total energy of $Pd_{31}Ru_1$ bulk alloy, and $E_{Pd_{32},\ bulk}$ is the total energy of Pd_{32} bulk. We considered Ru cation exchange reaction is more favorable than solvated $RuCl_3$ state when $\Delta E_{relative}$ is negative. Schematic illustration of the calculation are described in Fig. S46. The exchange reaction energy of PdCe and AuRu were calculated in the same manner as PdRu case (Figs. S32, S35).

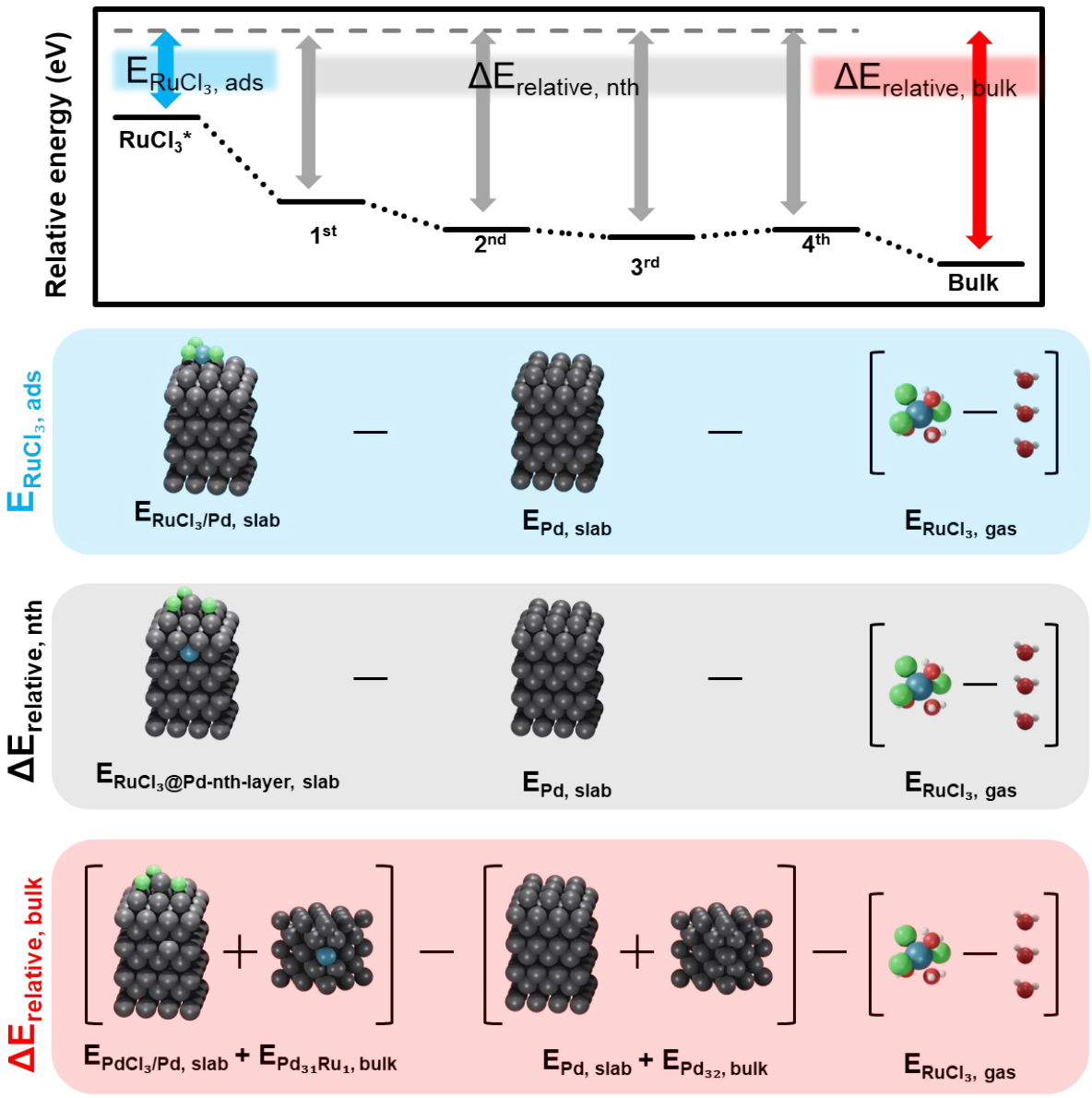

Fig. S46. Schematic illustration for DFT-calculated energetics of each steps of $RuCl_3$ exchange reaction on Pd(100), $E_{RuCl_3, ads}$, $\Delta E_{relative, nth}$, and $\Delta E_{relative, bulk}$. (Color code: Pd: dark gray, O: red, H: white, Cl: green and Ru: blue)